

Late Miocene Incision of the Salmon River:
Implications for the Timing and Driving Mechanisms of Topographic
Evolution of the Inland Northwest

A Thesis

Presented in Partial Fulfillment of the Requirements for the

Degree of Master of Science

with a

Major in Geological Sciences

in the

College of Graduate Studies

University of Idaho

by

Jeffrey E. Larimer

Major Professor: Brian J. Yanites, Ph.D.

Committee Members: William Phillips, Ph.D.; Elizabeth Cassel, Ph.D.

Department Administrator: Mickey Gunter, Ph.D.

May 2015

AUTHORIZATION TO SUBMIT THESIS

This thesis of Jeffrey E. Larimer, submitted for the degree of Master of Science with a Major in Geological Sciences and titled "Late Miocene Incision of the Salmon River: Implications for the Timing and Driving Mechanisms of Topographic Evolution of the Inland Northwest," has been reviewed in final form. Permission, as indicated by the signatures and dates below, is now granted to submit final copies to the College of Graduate Studies for approval.

Major Professor: _____ Date: _____
Brian J. Yanites, Ph.D.

Committee Members: _____ Date: _____
William Phillips, Ph.D.

Elizabeth Cassel, Ph.D.

Department Administrator: _____ Date: _____
Mickey Gunter, Ph.D.

ABSTRACT

Throughout the tributaries of the Salmon River watershed, there is an observable break in slope that separates low relief (<400m deep valleys) headwaters from the high relief (1200-1600m deep valleys) main stem of the Salmon River gorge. This transience was triggered by baselevel lowering along the Salmon River sometime during the late Cenozoic. However, the timing of the incision is unknown as is the mechanism that caused it. To provide insight into the drivers of landscape evolution in this region, we integrate field data with numerical modeling to constrain the timing of incision and gorge formation. We present ^{10}Be cosmogenic radionuclide concentrations from bedload sediment in ten different tributaries of the mainstem Salmon located between the South Fork and Riggins, ID. The samples record basin wide erosion rates ranging from ~ 0.05 mm/yr in low-relief topography to ~ 0.12 mm/yr in high-relief topography over the last 10^3 - 10^4 yrs. We use these erosion rates together with slope-area regression analysis to calibrate a 1D river incision model for rivers draining the Idaho Batholith rocks. After a suite of model runs we perform a best-fit analysis to constrain the timing and rate of baselevel change. The results suggest an increase in the incision rate of the Salmon River occurred roughly 8-10 Ma and has continued at a persistent rate. These results combined with other long-term exhumation rates of the region are consistent with a hypothesis that the increase of incision was initially driven by lithospheric delamination facilitated by the Yellowstone plume and then maintained by drainage capture following migration of the continental divide.

ACKNOWLEDGEMENTS

This research was supported by the University of Idaho Office of Research and Development. I would like to thank my committee members for their constructive comments, Bill Phillips for guidance through quartz separation, Greg Chmiel and Tom Clifton at PRIME Lab, Judy Totman Parrish for giving us a bird's-eye view over the Salmon River Gorge, Clay Sorensen for his help collecting samples, and especially Brian Yanites for his vision and leadership throughout the process.

TABLE OF CONTENTS

| | |
|--|-----------|
| Authorization to Submit Thesis | ii |
| Abstract..... | iii |
| Acknowledgements..... | iv |
| Table of Contents..... | v |
| List of Tables | viii |
| List of Figures | ix |
| CHAPTER 1: INTRODUCTION | 1 |
| 1.1 STUDY AREA | 4 |
| CHAPTER 2: METHODS | 6 |
| 2.1 TERRESTRIAL COSMOGENIC RADIONUCLIDE EROSION RATES | 6 |
| 2.1.1 Sample Preparation | 7 |
| 2.1.2 Erosion Rate Calculation..... | 7 |
| 2.1.3 Snow Shielding | 8 |
| 2.2 TOPOGRAPHIC METRICS..... | 11 |
| 2.2.1 Paleo-Profile Reconstruction..... | 13 |
| CHAPTER 3: RESULTS | 14 |

| | |
|---|-----------|
| 3.1 BASIN-WIDE EROSION RATES | 14 |
| 3.2 TOPOGRAPHIC ANALYSIS | 14 |
| CHAPTER 4: THE MODEL | 16 |
| 4.1 MODEL SETUP | 16 |
| 4.2 MODEL CALIBRATION..... | 17 |
| 4.3 MODEL WALK-THROUGH | 19 |
| 4.4 BEST-FIT ANALYSIS..... | 20 |
| 4.5 MODEL RESULTS..... | 21 |
| CHAPTER 5: DISCUSSION | 23 |
| 5.1 SALMON RIVER INCISION | 23 |
| 5.2 POSSIBLE TRANSIENT DRIVERS | 24 |
| 5.2.1 Capture of Lake Idaho..... | 24 |
| 5.2.2 Yellowstone Magmatism, Plume, and Hotspot..... | 25 |
| 5.2.2.1 <i>Columbia River Basalts</i> | 27 |
| 5.2.2.2 <i>Plume-Lithospheric Interaction</i> | 29 |
| 4.3 CAVEATS | 33 |
| 4.4 JUSTIFICATION FOR A DETACHMENT-LIMITED MODEL..... | 34 |

| | |
|------------------------------------|-----------|
| CHAPTER 5: CONCLUSION | 36 |
| REFERENCES | 38 |
| TABLES | 48 |
| FIGURES..... | 50 |

LIST OF TABLES

| | |
|--|----|
| Table 1: Basin characteristics | 48 |
| Table 2: The six different parameter sets..... | 49 |

LIST OF FIGURES

| | |
|--|----|
| Figure 1: Study Area | 50 |
| Figure 2: Major baselevel changing geologic events of the late Cenozoic..... | 51 |
| Figure 3: Snow cover corrections..... | 52 |
| Figure 4: Example model run..... | 53 |
| Figure 5: Model calibration..... | 54 |
| Figure 6: Basin averaged erosion rates | 55 |
| Figure 7: steepness profiles and elevation map..... | 56 |
| Figure 8: Example of X^2 misfit test | 57 |
| Figure 9: [A-C]: X^2 misfit results for each basin through all six parameter sets | 58 |
| Figure 10: Map of Columbia River Basalt | 59 |
| Figure 11: Evolution of the Yellowstone plume | 60 |
| Figure 12: The influence of flood basalts on the river profile..... | 61 |
| Figure 13: Plume-lithosphere dynamics..... | 62 |
| Figure 14: Continental divide migration from 9 Ma to the present..... | 63 |

CHAPTER 1: INTRODUCTION

Rivers respond to tectonic and geologic events that affect their baselevel and magnitude of discharge. The complex geological history of the Northern Rockies has undoubtedly influenced the evolution of river systems in the region (Link et al., 1999; Wegmann et al., 2007; Reidel and Tolan, 2013). For example, central Idaho and surrounding areas of the Inland Northwest are incised with deep canyons (figure 1a). The Salmon, Snake, and Clearwater Rivers draining central Idaho have incised some of the deepest canyons in North America, frequently exceeding 1.5 km in depth. However, the timing and driving mechanism of the incision of these canyons remain enigmatic.

In the past, the Inland Northwest has been recognized as a deeply dissected plateau in which the elevated 'peneplain' is the remnant of an old baselevel or erosion surface (Umpleby, 1912; Schofield, 1915; Ross, 1928; Anderson, 1929). The old erosional surface was assumed to be Eocene in age due to its relation to Miocene lakebeds and Eocene deposits. Umpleby (1912) proposed that the granitic Idaho Batholith initiated the cycle of erosion responsible for the Eocene surface. However, Blackwelder (1912) suggests the 'peneplain' to be much younger and probably post Middle Miocene, but concludes, "It should not be regarded as an index of Eocene age, and its exact chronological value will depend upon a more reliable future determination." Ten years later, Anderson (1929) concludes that Miocene uplift carved deep canyons, which were then back filled by Columbia River flood basalts and then incised again by larger streams.

Modern studies of topographic evolution in this region have been limited and estimates of change in erosion rates are focused near the margins of the elevated topography. For example, using apatite (U-Th)/He thermochronology, Vogl et al. (2014) found that exhumation likely increased by 3-fold between 11-8 Ma. Beranek et al. (2006) reconstructed drainage patterns using detrital zircon provenance. Others have constrained incision rates during the last 1 million year by dating river terraces in the Middle Fork of the Salmon River (Meyer and Leidecker, 1999).

Significant advances have been made that constrain the processes and timing of geologic events in the Inland Northwest. Many of these events have the potential to influence baselevel and water discharge along the rivers of central Idaho (figure 2). For example, as the Yellowstone Hotspot and plume migrated across southern Idaho from ~17 Ma to the present (Pierce and Morgan, 1992), it likely had an affect on mantle-lithosphere dynamics (Burov et al., 2007; Shervais and Hanan, 2009), river baselevel (Vogl et al., 2012; Wegmann et al., 2007), and the re-organization of spatially distributed drainage patterns in response to the transient topographic swell (Beranek et al., 2006; Link et al., 2011). The emplacement of Columbia River Flood Basalts from 17.5-6 Ma (Reidel et al., 2013) also have the potential to influence topographic evolution of the region. The basalts emerged from the Chief Joseph dike swarm at ~17 Ma and intermittently filled in low topography and valleys of the Columbia River drainage for the next eleven million years effectively raising baselevel along the rivers of central Idaho (figure 2). Finally, the draining of Lake Idaho sometime between 6.4 and 1.7 Ma (Perkins et al., 1998; Neville et al., 1979; Izett, 1981; Van Tassel et al., 2001; Smith et al., 2000; Othberg, 1994) could also

have influenced regional incision history. When the lake spilled over into the Snake River, the increase in discharge could have down-cut the riverbed and lowered the baselevel throughout the integrated Columbia River network. Any one of these events may have influenced the dynamics of erosion across the region through baselevel alteration. Determining which (if any) of these mechanisms is responsible for the canyon development in the Inland Northwest requires quantitative constraints on the incision history of the regional rivers.

In this study, we quantify the topographic response of eleven tributaries of the Salmon River to determine the timing of increased incision along the Salmon and consider the possible driving mechanisms of Late Cenozoic topographic evolution of the region. At some time in the past, incision along the Salmon River lowered the mouths of the adjoining tributaries, generating a wave of incision that has migrated upstream through the tributaries ever since. The timing of increased incision in the tributaries is therefore directly related to the incision history along the Salmon River. We present erosion rates from cosmogenic radionuclide concentrations as well as topographic metrics from a slope-drainage area analysis in tributaries between the South Fork of the Salmon and Riggins, ID figure 1b. We interpret these results using a calibrated 1D numerical model of transient river incision with the goal of simulating the evolution of river profiles through time. A best-fit analysis of the model results constrains the timing of the onset of deep canyon incision. We use the timing, magnitude, and rate of baselevel change with other published data to discuss the possible driving mechanisms behind the topographic evolution of central Idaho and the Inland Northwest.

1.1 Study Area

Throughout the Salmon River watershed, there is an observable break in slope that separates low relief (<400m deep valleys) headwaters from the high relief (1200-1600m deep valleys) main stem of the Salmon River gorge. The break in slope marks the headward advance of the transient boundary between low relief topography and high relief topography. Evidence of a transient wave of incision exists throughout much of central Idaho and is easily recognizable by the dichotomy of steep and gentle slopes that trace the mainstem river valleys (figure 1c), including the Snake River through Hell's Canyon, the Salmon River, and the Clearwater River. Observations of canyon depth show that this transient morphology decays downstream of Lewiston (figure 2), but not before it cuts through 11 m.y. of Columbia River Basalt emplacement.

Between the South Fork of the Salmon and ~20 km upstream of Riggins, Idaho, the Salmon River incises into Idaho Batholith granodiorites and tonalites. The quartz-rich nature of this rock provides an opportunity to quantify erosion rates using cosmogenic nuclides (Granger et al., 1996). We classify the study area into three landscape types of basins based on their topography: 'relict' (low-relief landscape yet to be incised), 'adjusted' (high-relief landscape that has been incised), and 'transient' (contains both low relief and high relief landscape separated by a migrating knickpoint) (figure 1c). We focus our analysis on basins ranging from 1-10³ km² that include each landscape type and are primarily underlain by Idaho Batholith granodiorites and tonalites.

We selected a series of tributary basins and sub-basins as our focused study locations. These sites were selected to provide a range of landscape types (relict, adjusted, and transient) as well as a range of drainage areas. Within these sites there are four relict basins (Upper Fall Creek, an unnamed stream near Burgdorf, an unnamed stream near Chinook Campground, an unnamed stream off of Secesh Road), one adjusted basin (Longtom Creek), and five transient basins (Fall Creek, French Creek, Pony Creek, South Fork, and Carey Creek). Additionally, our study area is near previous work by Kirchner et al. (2001) who sampled cosmogenic nuclides in detrital sand at two adjusted basins (Tailholt Creek and Circle End).

CHAPTER 2: METHODS

The framework for our methodology is focused on calibrating a river incision model. Because incision history is unknown along the Salmon River, we seek to test different baselevel lowering histories for the adjoining tributaries. To do this we will model different tributary incision histories to see what scenario best predicts the modern longitudinal profiles. We focus model simulations on tributaries where the transient signal has not yet worked its way through the system. We do this for two reasons: (1) it allows reconstruction of a paleo-river profile from the relict topography (Clark et al., 2005), which we use as a starting point for the river incision model and (2) the ability to reproduce the location of the knickpoint is important to distinguish between different modeled scenarios. The calibrated erosion model requires estimates of erosion rates and topography in both the relict and adjusted portions of the landscape.

2.1 TERRESTRIAL COSMOGENIC RADIONUCLIDE EROSION RATES

We use the concentration of the terrestrial cosmogenic nuclide ^{10}Be in fluvial sediments to determine how erosion rates vary in both relict and adjusted topography. Cosmogenic nuclides in stream sediment record the average time taken to lower the surface of the landscape upstream of the sample point by the depth of the cosmic ray mean free path. This approach yields a spatially averaged erosion rate of the basin integrated over 10^2 to 10^5 yrs (Brown et al., 1995; Granger et al., 1996; Biermann and Steig, 1996). Inferring erosion rates from bedload sediment can be confounded by shielding of bedrock by snow (Schildgen et al., 2005), recent

landslides (Yanites et al., 2009), glaciation, significantly long storage time (Biermann and Steig, 1996), and unequal distribution of the mineral being analyzed (Brown et al., 1995). To avoid these pitfalls we chose catchments that did not display signs of significant landslides, glaciation, or changes in lithology, with the exception of two (see discussion). Due to the relatively steep gradient and lack of thick cover of sediment in the streams, sediment storage times are likely much less than the resident time of rock in the cosmic ray attenuation zone and can therefore be ignored.

2.12 Sample preparation

The samples were wet sieved to separate the 250 to 500 microns grain size fraction. In general, our lab procedure for quartz isolation followed that of Kohl and Nishuziimi (1992) with a few modifications. Quartz was isolated through a series of steps including: an etch in HCl, four leaches in dilute HF/HNO₃, heavy liquids separation in Lithium Metatungstate, and magnetic separation. Each sample was then dosed with known amounts of ⁹Be. Beryllium was isolated from other elements through cation exchange columns, precipitated as beryllium hydroxide, oxidized to BeO, mixed with niobium powder, packed into sample holders, and ratios of ¹⁰Be/⁹Be were measured at PRIME Lab at Purdue University.

2.13 Erosion rate calculation

¹⁰Be accumulates in rock primarily through neutron spallation and muon capture, and the amount of accumulation depends on time of exposure to and production rate by cosmic rays (Lal, 1991). Attenuation of cosmic rays decreases exponentially with

depth, and the rate at which rocks are eroded through the upper two meters of the Earth's surface (E) is reflected in the cosmogenic nuclide concentration (N) (Lal, 1991).

$$E = \left[\left(\frac{P_0}{N} \right) - \lambda_{\text{Be}} \right] \frac{\Lambda}{\rho_b}, \quad [1]$$

where P_0 is the neutron and muon production rate at the surface (atoms/yr), N is the ^{10}Be concentration (atoms/g), λ_{Be} is the decay constant (4.997×10^{-7} 1/yr (Chmeleff et al., 2010)), Λ is the effective attenuation length of cosmic ray flux at the Earth's surface (160 g cm^{-2} (Gosse and Phillips, 2001)), and ρ_b is the density of bedrock (2.65 g cm^{-3}). The concentration of ^{10}Be (N) in each sample was calculated from the ratios of $^{10}\text{Be}/^9\text{Be}$ measured by accelerator mass spectrometry. Nuclide production rates for each basin were calculated pixel by pixel from a 10 m DEM (USGS National Elevation Data) while correcting for latitude and elevation using methods from Hidy (2013). This resulting erosion rate is the spatially and temporally averaged erosion rate of the entire basin over the duration of the time it took to erode the upper two meters of rock (10^2 to 10^5 yrs).

2.14 Snow shielding

Snow cover attenuates cosmic rays thereby preventing them from reaching the underlying bedrock. This reduces the nuclide concentration in bedrock and falsely increases the apparent erosion rates derived from cosmogenic nuclide concentrations. Shielding corrections for snow cover have been approached in a variety of ways, often resulting in a $> 10\%$ correction in cosmogenic erosion rates for mountainous, mid-latitude regions (Schildgen et al., 2005). Our method uses

elevation data to model the magnitude and effects of snow cover on the nuclide production rate. We take modern snow cover data from different elevations near the study area to determine a relationship between snow cover and elevation. We use this relationship to infer snow cover over the duration in which cosmic rays were attenuating in our samples (4 to 13 ka). However, this time period includes a climatic shift during the last glacial maximum (LGM) in which snow cover was likely affected by colder temperatures.

The study area spans over 2000m in elevation leading to a significant temperature gradient and variable snow cover. The depth of snow cover varies significantly from lower elevations to higher elevations. The reduction in cosmic ray spallation in bedrock by snow cover depends on the depth and density of the overlying snow. We quantify the impacts of snow cover by calculating the nuclide production rate at the snow-bedrock interface with the depth dependent exponential production profile model

$$P_s = P_0 e^{-\left(\frac{s}{\lambda}\right)}, \quad [2]$$

where P_s is the production rate at a shielding depth s (g cm^{-2}). The shielding depth is calculated as the product of the depth of snow cover and the density of snow, also referred to as snow water equivalency. It follows that the fraction (F) of cosmic rays attenuated by snow cover or the shielding factor is

$$F = 1 - e^{-\left(\frac{s}{\lambda}\right)}. \quad [3]$$

Monthly averages of climate data since 1940 show that snow cover is rare at the elevation of the tributary mouths, averaging one inch of snow depth for the month of January (Western Regional Climate Center, Riggins, ID (107706)). However, snow cover is significant at the elevation of the headwaters, lasting from November to June and reaching snow water equivalency depths of 78cm during peak snow season (Western Regional Climate Center, NRCS SNOTEL). We use the water equivalency data of four nearby SNOTEL sites to calculate the 32 year mean snow cover attenuation fraction. Figure 3 shows the dependence of snow shielding to elevation at these four sites. Using this relationship each pixel in the DEM is given a 'fraction of snow attenuation' based on its elevation.

Before we can update the nuclide production rate, we must also account for possible temporal variations in snow cover due to long-term climate change. The difference in erosion rate (see RESULTS below) between relict and adjusted landscapes results in differences in residence time of rocks in the nuclide production zone (relict ~13000 yrs and adjusted ~4000 yrs, see results below). Because climate has changed on a similar time scale to the residence times, we consider potential biases that could result from temporal variations in snow cover.

We calculated the magnitude of snow shielding for each pixel in the DEM by taking the pixel's elevation dependent shielding factor and averaging it over the duration of its residence time. For pixels in the faster eroding adjusted landscape, we assume negligible climate change over the last 4000 yrs and use the modern relationship of snow shielding with elevation throughout the residence time duration. For pixels in the relict landscape, we estimate the effects of a cooler climate on snow

cover by reducing the y-intercept of the regression line (FIGURE 3). To adjust the intercept, we need to pin an elevation to a particular attenuation fraction. We note that during the LGM, glaciers extended down to ~2300m in the region. In most glaciated terrains, the steep valley walls are subject to frequent snow avalanching, exposing rock for much of the year. We assume that the exposed rock is ~1/3 of the landscape and 2/3 is covered by deep snow and ice. Therefore, in steep glaciated terrain (~2300m during LGM for our study area), 2/3 of the incoming cosmic rays were attenuated by the snow and ice. We use this fraction and elevation to lower the regression line on figure 3 for the LGM. Within the model run we begin adjusting the intercept from our modern relationship at 9 ka so that by 12 ka the minimum elevation of Pleistocene glaciated terrain in the study area (~2300m) is at 0.66 snow shielding. To determine which residence time a pixel should be modeled over, we designate the pixel as relict or adjusted based on its position relative to the transient signal. Each basin's nuclide production rate is adjusted according to the mean correction factor among all pixels in the basin.

2.2 Topographic Metrics

Next we analyze topography to determine the relationship between channel slopes and erosion rates. This relationship will allow us to calibrate an erosion model that is specific to our study area. We calculate a channel steepness (k_s) index for each analyzed tributary basin for two reasons: (1) to determine both the location of the boundary between relict and adjusted domains of the river profile (i.e. identify the knickzone) and (2) to quantify the slope differences between relict and adjusted landscapes. The channel steepness index represents the channel slope normalized

by the contributing drainage area raised to a reference concavity (Wobus et al., 2006). Because channel slopes tend to decrease with increasing drainage area, this normalization by area allows a comparison of river slopes with different upstream drainage areas. Steepness is calculated by extracting the elevation, flow distance, and upstream contributing drainage area along each tributary stream and is expressed by a power-law function (Hack, 1973, Flint, 1974, Howard and Kerby, 1983):

$$k_s = SA^\theta, \quad [3]$$

where S is the local slope, A is the contributing drainage area at each point along the profile, and θ is the concavity index. Values of k_s and θ are found by regressing the log-transformed slope and area values along a stream. In order to compare different sized basins we normalized k_s with a reference concavity (Wobus et al., 2006):

$$k_{sn} = SA^{\theta_{ref}}. \quad [4]$$

A reference concavity is an assumed concavity that imposes a slope on the regression on the log-log plot. This means that an increase in slope with distance downstream will result in a distinct spike in the k_{sn} value. The spike in k_{sn} enables relict and adjusted domains of a channel to be easily distinguished and the values of k_{sn} can be compared among the other drainage basins in the study area. We chose a reference concavity based on the regional mean of observed relict concavities.

We extracted elevation data from a 10m DEM (USGS National Elevation Data) for each drainage basin, which is delineated by the contributing drainage area

upstream of each cosmogenic sample site. River profiles were obtained by calculating flow direction in ARCGIS software, and using MATLAB scripts to follow the path of pixels downstream while recording elevation, streamwise distance, and contributing drainage area data. Elevation data of the profiles were smoothed by a 55 pixel (550m) moving window average. This was done to remove inherent noise in the river profile (Wobus et al., 2006). We calculated the steepness index at each node along the stream profiles (equation 4). We then isolated the transition zone from low to high steepness index to determine the location and elevation of knickpoints. The knickpoint is a downstream shift from concave up to concave down, and can be pinned to an objective location among the drainage basins by identifying where the 2nd derivative of the stream profile equals zero.

2.21 Reconstructing Paleo-Profiles

The paleo-profile is the theoretical reconstruction of the tributary profile prior to incision. Reconstruction of the paleo-profile provides us with both a starting point for our model runs as well as an estimate of the total amount of river incision below the relict landscape (figure 4). We determined the local concavity and steepness of the relict portions of each tributary by fitting a power-law relationship to their slope-area data with θ and k_s as free parameters. For each transient basin that we modeled, a paleo-profile was recreated by calculating the theoretical slope at each node with equation 3. For A in equation 3, we use values of drainage area that we derive from the DEM assuming no significant change in drainage area from when the relict landscape began adjusting to the present.

CHAPTER 3: RESULTS

3.1 COSMOGENIC EROSION RATES

There is a 2.4-fold increase in erosion rate between the relict and adjusted landscapes. Erosion rates ranged from 0.05 ± 0.005 mm/yr to 0.08 ± 0.01 mm/yr in the relict landscape and 0.11 ± 0.01 to 0.15 ± 0.02 mm/yr in the adjusted landscape (table 1), with averages of 0.065 and 0.13 mm/yr respectively. After we corrected for snow shielding these rates dropped to an average of 0.05 ± 0.008 mm/yr and 0.12 ± 0.02 mm/yr respectively (figure 6). Snow shielding corrections reduced erosion rates by 23% in relict landscapes and less than 10% in adjusted landscapes. Our snow-corrected erosion rates agree with the 0.02-0.12 mm/yr cosmogenic denudation rates from other nearby sites in the Idaho Batholith from (Kirchner et al., 2001; Ferrier et al., 2011).

3.2 TOPOGRAPHIC ANALYSIS

There is a 3.8-fold increase in steepness index between the relict and adjusted landscapes. Mean relict steepness is 80 ± 36 standard deviation and increases to 300 ± 80 in the adjusted landscape (table 1). Steepness profiles of each basin are shown in figure 7. The transition from warm to cool colors roughly indicates the location of the knickpoints. Four out of five knickpoints are within 184 meters elevation of each other (average 1800 m), while the knickpoint in French Creek is 1190m in elevation (see discussion of French Creek below). These four knickpoints more or less have a spatially uniform vertical velocity, which is consistent with a detachment-limited model (Niemann et al., 2001), where the vertical velocity of

knickpoints relative to the confluence with the Salmon is independent of drainage area and slope and only depends on uplift rate and erosion physics.

Both French Creek and the South Fork deviate significantly from the other transient basins (table 1). Upon further inspection, French Creek and the South Fork display evidence of recent landslides and significant glaciation. This undoubtedly confounds the erosion rates and the shape of the profiles (see DISCUSSION below). Therefore, we removed French Creek and the South Fork from the above topographic analysis and focused the model runs on the three applicable transient basins: Fall Creek, Pony Creek, and Carey Creek.

CHAPTER 4: THE MODEL

4.1 MODEL SETUP

The purpose of our model is to determine the time it has taken for the transient signal to migrate from the tributary mouths to their current locations within the transient basins using a field calibrated, 1D river profile model. In our modeling framework, the length of time since the Salmon River began the period of increased incision is referred to as the run duration (or the amount of time between the initiation of canyon incision and the present). Therefore, the run duration of the model run that best predicts the shape of the modern river profile is the timing of when incision along the Salmon began. We explore different rates of the incision pulse allowing for scenarios in which the elevation of the paleo-Salmon reaches the modern elevation well before the present. When this occurs, we assume the Salmon returns to eroding at the rate of uplift (relict erosion rate) and baselevel is held constant until the end of the run duration (i.e., until 0 Ma). The fraction of incision pulse is the amount of time it takes for the mouth of the tributary to incise from the paleo-reconstruction to the modern elevation. We describe this length of time by the fraction of run duration so that the run duration can be 1 m.y. or 20 m.y. and we are able to test a full range of incision pulse time-lengths for all model runs. For example, a fraction of run duration = 1 means that the pulse of incision has continued until modern day. In the case of a run duration of 10 m.y. and fraction of 0.1, the pulse of incision began 10 Ma and lasted for only 1 m.y. (i.e. by 9 Ma, the

Salmon was at the modern elevation and remained in equilibrium for the remainder of the run duration incising at the rate of rock-uplift).

The change in elevation over time at each node along the river profile is determined by

$$\frac{\partial z}{\partial t} = U - E, \quad [5]$$

where U is spatially uniform rock-uplift and E is erosion. For rock-uplift rate, we use the erosion rate of the relict landscape, which we will show does not influence the model results because the transient pulse of incision is dictated by the relative baselevel/elevation change. To calculate erosion at each node we use the slope-area proxy equation (frequently referred to as the 'stream power equation')

$$E = KA^m S^n, \quad [6]$$

where K is the rock erodibility, and m and n are exponents that depend on the hydraulic control on bedrock erosion (e.g. unit stream power or shear stress (Whipple and Tucker, 1999)). In steady state it can be shown that m and n control the river concavity with

$$\theta = \frac{m}{n}. \quad [7]$$

This provides an important connection between our topographic analysis and model parameterization.

4.2 MODEL CALIBRATION

In order to constrain the unknowns of equation 6 (K , m , and n) we use the covariance between the cosmogenic erosion rates and channel steepness indices. Throughout the landscape there is a 3.8-fold increase in the mean steepness from relict to adjusted landscape that is matched by a 2.4-fold increase in the mean erosion rate. Assuming that slope is the dominant control on erosion rate in the study area (i.e. channel width variations are negligible), the relationship between channel steepness (k_s) and erosion rate provides a means to calibrate n . To estimate n we use a logarithmic regression of erosion rate to steepness:

$$n = \frac{\log(\Delta E)}{\log(\Delta k_{sn})}. \quad [8]$$

This suggests that $n=0.66$ and is consistent with a shear stress model of river incision (Howard and Kerby, 1983), which provides further confirmation that a detachment-limited model is applicable within these tributaries of the Salmon River. This is our preferred n , but we also dedicated a suite of model runs to $n=1$, which corresponds to the unit stream power model (Whipple and Tucker, 1999). We calculate m with equation 7 by using the regional mean observed concavity of the relict topography. We now have a value for m and n that is representative of our study area. Using equation 6 we can insert slope, area, and erosion rate and solve for K .

For the simulation of each transient basin we try different n values (0.66 and 1) and different relict cosmogenic erosion rates (minimum, mean, and maximum ranging from 0.035 to 0.063 mm/yr (table 1)) producing six different calibrated parameter sets. Each time we change n and relict erosion rate, the values for m and

K are recalculated accordingly. The values for relict erosion rate, K, m, and n within the six different parameter sets are shown in TABLE 2.

4.3 MODEL WALK-THROUGH

A landscape reaches steady-state when the erosion rate has matched the rock-uplift rate and there is no change in surface elevation (Gilbert, 1909; Hack, 1960). The relict erosion rate reflects steady-state conditions of the past because the relict profiles are smooth, concave-up, and show no significant change in steepness or concavity. Therefore, we use the relict erosion rate for U (rock-uplift) in equation 5 and hold it constant throughout the simulation. An example simulation begins with the paleo-profile in steady-state, which means the entire profile is being uplifted and down-cut at the same rate, effectively holding elevation at each node stationary. At time step one we initiate canyon incision by dropping baselevel (the elevation of the end node of the tributary). This corresponds to when the pulse of incision along the Salmon River began passing by the tributary mouth. With the tributary mouth now down-cutting at this increased rate, the local slope just upstream of the mouth is increased. According to equation 5 an increase in slope drives an increase in erosion, and an upward convexity or knickpoint begins migrating upstream along the tributary. Throughout the remaining time steps, the baselevel of the tributary continues dropping incrementally until it has reached the modern elevation. In this configuration the elevation of the relict topography is held constant while the Salmon River down-cuts. In an alternative scenario, the elevation of the Salmon River is held constant while the surrounding landscape uplifts. In practice both of these scenarios have the same end result because the transience is controlled by the relative

change in baselevel between the Salmon River and the relict topography. Without knowing paleo-elevation we cannot distinguish between which mechanism, uplift or down-cutting, produces the transience.

We use the three applicable transient basins to constrain the date of initial incision by performing a suite of model runs through all six parameter sets that vary with run duration and fraction of incision pulse. We test run durations from 1-20 million years in increments of one million years and fraction of the rate of incision pulse from 0-1 in increments of 0.5.

4.4 BEST-FIT ANALYSIS

To evaluate the accuracy of simulated incision histories we use the X^2 misfit function (Jeffery et al., 2013). We compare the resulting river profile to the modern river profile and estimate the misfit

$$X^2 = \frac{1}{N-\nu-1} \sum_i^N \left(\frac{\text{sim}_i - \text{obs}_i}{\text{tolerance}} \right)^2, \quad [9]$$

where N and ν are the number of nodes along the profile and free parameters in the model run, sim_i is the simulated elevation, and obs_i is the observed elevation smoothed over 550 m of points. The tolerance is the standard deviation of the differences between the observed relict profiles from the pre-model reconstructed relict profiles. We measure this by comparing the relict domain of the smooth theoretical paleo-profile (calculated with equation 3) to the noisier observed relict domain. The maximum standard deviation between theoretical and observed relict profiles was 30m. Therefore, by using a tolerance of 30m, a X^2 misfit value of ≤ 1

means that average difference between profiles is under 30m, and a value ≤ 2 is within 60m.

4.5 MODEL RESULTS

Figure 8 is an example of two X^2 misfit analyses using parameter sets (2) and (5) (table 3) for 400 model runs of different run durations (1-20 m.y.) and different fractions of incision pulse (0.1-1). The smallest degree of misfit for all basins occurs when the incision pulse is spread evenly over the entire run duration. This suggests that the pulse of incision along the Salmon has been persistent during gorge formation, meaning that down-cutting along the Salmon continues today.

Figure 9 shows the timing of increased incision, X^2 value, and incision rate for the interpolated best-fit simulations with a persistent incision rate. Incision rates are calculated from the summation of baselevel change below the relict landscape and total relict erosion/rock-uplift throughout the run duration. Plots A-C show the results for the six different parameter sets used to model the three applicable transient basins. The shear-stress model parameter sets ($n=0.66$) consistently yield better misfit values than the stream power per unit bed area model parameter sets. The shear stress model also produces incision rates that are closer to the mean erosion rate of the adjusted landscape (0.12 mm/yr).

The use of minimum and maximum relict erosion/rock-uplift rates constrains a range of possible timings. The stream power per unit bed area model constrains a timing of 4.7 Ma with a standard deviation across all best-fits of ± 1.4 m.y., while the shear-stress model constrains a timing of 10.0 ± 2.7 Ma. The results of the 2nd

parameter set (table 2), which uses the mean relict erosion/rock-uplift rate, show that the pulse of incision reached the tributaries in our study area from 8-10 Ma constrained by the minimum and maximum timing. This parameter set uses our mean relict erosion rate, which is consistent with erosion rates from other studies in relict landscape near our study site (Kirchner et al., 2001; Ferrier et al., 2011).

CHAPTER 5: DISCUSSION

5.1 SALMON RIVER INCISION

Based on the best-fit modeling and preferred calibrated parameter set ($n=0.66$, mean relict erosion/rock-uplift rate= 0.05mm/yr , $K=2.76\times 10^{-6}$), we estimate a ~3-fold increase in Salmon River incision occurred ~8-10 Ma, and has been incising at a persistent rate on the order of 0.12 to 0.15 mm/yr. We note that the modeled incision rate (0.15 mm/yr) is slightly faster than the cosmogenic erosion rate (0.12 mm/yr), however, this is within error.

Our timing of increased incision and magnitude of erosion rates are consistent with other work from the local to regional scale and measured over longer time scales (e.g. Meyer and Leidecker, 1999; Sweetkind and Blackwell, 1989; Vogl et al., 2014). In adjusted landscape along the Middle Fork of the Salmon, average incision rates have been estimated from river terraces to be between 0.12-0.16 mm/yr since 1.1Ma (Meyer and Leidecker, 1999). Moreover, this continued incision since 1 Ma along the Middle Fork is consistent with our modeled finding of a persistence in the increase in erosion along the Salmon River.

Our relict erosion rates are consistent with long-term exhumation measurements from the region. Fission-track data from the Idaho Batholith (Sweetkind and Blackwell, 1989) suggest erosion rates were 0.03-0.1 mm/yr from ~50-10 Ma and underwent a 3-fold increase beginning at 11.4 ± 1.4 Ma in. Furthermore, 170 km south of our field area in the Pioneer-Boulder Mountains, Vogl et al. (2014) found exhumation rates to significantly increase beginning between 11-8 Ma following a

long period of little to no exhumation. These dates of increased incision from spatially diverse areas of central Idaho are concordant with our study and suggest the entire region of central Idaho experienced a shift in incision rates at approximately the same time.

5.2 POSSIBLE TRANSIENT DRIVERS

We now consider the timing of initial incision (~8-10 Ma) and the persistent nature of the incision pulse with respect to three major geologic events occurring during the late Cenozoic in the inland Northwest. These events have the potential to influence river baselevel throughout the region and generate pulses of incision. By comparing our findings with the timing of these events, we hope to illuminate major drivers of Miocene to present landscape evolution in the Inland Northwest.

5.2.1 Capture of Lake Idaho

Ancient Lake Idaho formed in the wake of the Yellowstone Hotspot. During its existence from 10.1-6 Ma it filled most of the Western Snake River plain (figure 2) (Wood and Clemens, 2002). Previous studies have suggested that the lake catastrophically spilled over into the Snake River sometime between 6.4 and 1.7 Ma, integrating the Snake River Plain into the Columbia River drainage system (Wood and Clemens, 2002). This integration increased the Snake River's drainage area downstream of the spillover point by several orders of magnitude. Such an event can generate a pulse of incision downstream of the spill-over point that transmits to the other rivers within the network (Yanites et al., 2013). We discount this scenario

because the timing of increased incision along the Salmon pre-dates the constrained timing of over-spill of Lake Idaho (6.4-1.7 Ma).

However, it is possible that the same transient pulse of incision that occurred along the Salmon 8-10 Ma also played a role in capturing Lake Idaho. The proto-Snake River likely experienced the same baselevel fall as the Salmon and Clearwater systems, driving a pulse of incision up this small drainage. This pulse of incision may have driven the migration of the drainage divide (Willet et al., 2010) between the proto-Snake and Lake Idaho. Because of the smaller drainage area of the proto-Snake, we would expect the transient wave of incision to require more time to work its way up the proto-Snake than in the bigger Salmon River. The pulse of incision arrived at our study area on the Salmon roughly 160 km upstream of the confluence at ≥ 8 Ma. The projected spillover point of Lake Idaho (Wood and Clemens, 2002) is roughly 210 km upstream of the confluence of the Snake and Salmon, and would have arrived there sometime between 6.4-1.7 Ma. Therefore, it appears that the pulse of incision arrived at Lake Idaho between ~2-8 m.y. after it arrived at our study area because it had a longer distance to travel and the paleo-Snake River was likely smaller in drainage area than the paleo-Salmon.

5.2.2 Yellowstone Hotspot and Related Volcanism

It is widely thought that the Yellowstone Hotspot marks the interaction between a rising mantle plume and the overriding North American Plate (Morgan, 1972; Pierce and Morgan, 1992; Camp and Ross, 2004; Jordan et al., 2004; Hooper et al., 2007). The main-phase of the Columbia River Basalt (CRB) eruptions was coeval with the

emergence of the Yellowstone hotspot roughly 16.7-15.6 Ma (Barry et al., 2010; Camp et al., 2013). However, the flood basalts emerged from dike swarms located 400km to the North of the proposed initiation of the Yellowstone Hotspot track at the McDermitt volcanic field.

A study by Shervais and Hanan (2008) presents a hypothesis that explains how a mantle plume could be responsible for both the CRBs and Yellowstone Hotspot track (figure 11). Their model accounts for the influence of lithospheric topography on the deflection of mantle plumes and unravels the spatial-temporal relationship of the CRBs and the hotspot track. In their model the plume head impacted the base of the lithosphere at 17 Ma under east central Oregon at $\sim 44^{\circ}\text{N}$, but west of the suture zone between the North American Craton and the oceanic terranes accreted to North America during the Mesozoic. As the lithosphere overrode the stationary plume, the plume head was flattened against the thick mantle root of the North American Craton and extruded to the north and south along the leading edge of the North American Cratonic root. The northern extrusion was responsible for the main phase Columbia River Basalt eruptions, which get younger to the north (Camp and Ross, 2004), suggesting a time-transgression caused by the northward extrusion. The southern extruding plume head followed a path under thinner cratonic lithosphere until it was eventually compressed against thick cratonic lithosphere culminating in the Breneau-Jarbridge eruptive center $\sim 11.5\text{-}8\text{Ma}$ (Bonnichsen, 1982). In summary, the base of the plume stem at 500-600 km depth has been located under central Idaho and western Montana ($\sim 44^{\circ}\text{N}$), while part of the plume head was diverted to the north leading to the CRB eruptions and part of the head was diverted

to the south with the stem following to the south. Recent seismic tomography provides support for this model as the plume stem remains in this position (plunging ~60° WNW) today under western Montana (Yuan and Dueker, 2005; Smith et al., 2009).

5.2.2.1 Columbia River Basalt Emplacement

From 17.5-6 Ma a total volume of 210,000 km³ of basalt emerged from the Steens Mountains and Chief Joseph dike swarm and flowed west from near the confluence of the Snake and Salmon into the Columbia River Basin (Reidel et al., 2013). Sections of basalt up to 1.2 km thick remain near Whitebird, ID and sections 3.2km thick remain in Pasco Basin (figure 10).

During this time, from 17.5 to 6 Ma, CRBs intermittently filled the valleys of the Columbia River Drainage system thereby providing a means to raise baselevel with each significant eruption; however the additional mass added to the crust would have generated subsidence. In relation to our timing of increased incision 8-10 Ma, we consider the timing and volume of basalt emplaced during the main phase eruptions and the lead up to cessation.

The main phase of CRB eruptions emplaced 206,000 km³ of basalt from 16.8-15.6 Ma (figure 10). During the waning phase the Saddle Mountains Basalt (SMB) eruptions emplaced 2,400 km³ of basalt from 15-6 Ma (Barry et al., 2013). SMBs are exposed throughout the lower Salmon River and Clearwater Basins and range in total thickness of 120-240m (Camp and Hooper, 1981). The Ice Harbor Member of the SMBs was emplaced during the last significant eruption ~8.5 Ma, in which it is

estimated that 75 km³ of basalt was emplaced (Reidel et al., 2013). This coincides with our date of initial incision along the Salmon River.

We propose a scenario in which incision rates prior to 17 Ma likely resembled modern rates (~0.15 mm/yr), and the emplacement of CRBs from 17.5-8.5 Ma raised baselevel throughout the Columbia River drainage (figure 12). This rise in baselevel is responsible for slowing erosion to 0.05 mm/yr and creating the gentle topography of the relict landscape. At the cessation of significant eruptions (IHBs ~8.5 Ma), baselevel begins to lower via erosion through the emplaced basalts and the pulse of incision migrates upstream into the relict landscape.

We now compare this rise in baselevel scenario to previous studies that have constrained a long-term erosion record. Combining ⁴⁰Ar/³⁹Ar cooling age measurements (Lund et al., 1986) 50 km north of our study area with a 25° C geothermal gradient (Sweetkind and Blackwell, 1989) shows that exhumation rates were 2.4-5.6 mm/yr shortly after emplacement of the Idaho Batholith 81-87 Ma, and slowed down to an average of 0.14 mm/yr from 67-54 Ma (Ferrier et al., 2012). If these incision rates persisted from 54 to 17.5 Ma then it strengthens the rise in baselevel hypothesis. However, such a persistence of erosion should result in younger AFT ages on the modern surface, but this is not the case in the Idaho Batholith (Lund et al., 1986; Sweetkind and Blackwell, 1989), which suggests slow erosion since 54 Ma (0.03-0.1 mm/yr).

Mapping of basalt stratigraphy shows that shortly following emplacement, the Snake River system frequently cut down into the basalt, evidenced by

unconformities and channelized fluvial gravels within the flow stratigraphy (Reidel et al., 2013). This suggests the paleo-river system quickly responded to emplacement of the lava flows. Furthermore, the subsidence rate of the Columbia River Basin during the emplacement of Saddle Mountain Basalts (15-8.5 Ma) was ~ 0.03 mm/yr (Reidel et al., 2013) while the maximum thickness of SMB (240 m) emplaced over 6.5 m.y. generated baselevel rise on the rate of 0.04 mm/yr. Therefore, subsidence alone negated nearly all baselevel rise, and emplacement of basalt could not have slowed incision from 0.15 mm/yr to 0.05 mm/yr over 6.5 m.y., as suggested in this scenario.

The eruptions of these basalts certainly influenced baselevel on these river systems over short timescales. However, combining the thermochronology data with evidence of quick incision response time, and a subsidence rate that was near the basalt thickness emplacement rate, we suggest that these impacts are of minor importance and cannot explain the persistent 3-fold increase in Salmon River incision since 8-10 Ma.

5.2.2.2 Plume-Lithosphere Interactions

The Yellowstone plume also has the potential to generate regional uplift through interactions between upwelling mantle material and the North American lithosphere. We now use the model proposed by Shervais and Hanan (2008) to consider a scenario in which the Yellowstone plume facilitates lithospheric delamination.

Burov et al. (2007) have shown that mantle lithosphere often delaminates along the leading edge of an expanding plume. Delamination of a dense crustal root has

been suggested to result in isostatic uplift as the effect of the positive buoyancy of the thickened crust overcomes the effect of the negative buoyancy of the detached mantle lithosphere (Valera et al., 2011). Figure 11 shows the cross section view of the spreading plume head, and figure 13a shows the map view of the time-transgression of the evolving plume (Shervais and Hanan, 2008). Tomographic images along a NW-SE transect show high P-wave velocity zones on the south side of the low velocity zone that follow the plunge of the plume stem (figures 13b & d). These high velocity zones are interpreted as down-welling mantle lithosphere from delaminated cratonic lithosphere (Yuan and Dueker, 2005). This interpretation combined with projected path of the tilted plume model from late Miocene plate motion suggests that lithospheric delamination has been an ongoing process related to the Yellowstone plume and could be the primary mechanism driving baselevel change in central Idaho. In this scenario, uplift generates a wave of incision that would work through the affected river systems.

The exact timing of initiation of delamination is not clear, but we can constrain it to sometime between 17-8 Ma by the dates of the appearance of CRB eruptions and the Breneau-Jarbidge eruptive center, which is associated with the culmination of the southern extension of the spreading plume head beneath thinned lithosphere. This window of time does overlap with our date of increased incision. Moreover, our study site is located farther to the east from the plume impact zone at the edge of the cratonic lithosphere. Therefore, a surface response at our site would occur later (i.e. closer to 8 Ma).

To consider a broader regional incision pattern that would result from a broad mantle delamination event, we calculate incision along the Selway River, a major tributary of the Clearwater that is north of our study area. To calculate incision rates along the Selway, we scaled down the magnitude of Salmon incision rates in proportion to the difference in canyon depths between the Salmon and Selway assuming similar timing of the initiation of canyon formation. When combined with other regional exhumation histories (Vogl et al., 2014), we are able to piece together an incision pattern in central Idaho that initiated 8-11 Ma (figure 13c). Vogl et al (2014) calculated incision rates of 0.3 mm/yr on the southern flank of the high topography of central Idaho (44°N). This is roughly the same latitude that corresponds with where the Yellowstone plume directly collided with the overriding North American Craton, and is perhaps where the most significant uplift occurred (figure 13a). We suggest the lower incision rates and surface elevation to the north, away from the southern flank of uplifted terrain, is caused by the signal of uplift decaying with distance from the focal point of delamination.

The likelihood of rock-uplift sustaining over a period of 8-10 m.y. as a result of delamination is difficult to reconcile, as basic aspects of continental delamination and topographic response remain unresolved (Valera et al., 2011). Additional factors include continued mantle upwelling balanced by lithospheric downwelling to maintain rock-uplift, a regional isostatic response to heightened erosion that maintains rock-uplift near the erosion rate set off by delamination, or continued basin growth through drainage reorganization. We favor a hypothesis in which delamination is responsible for the main pulse of incision, but not all of the incision.

We suggest that in the absence of continued mantle upwelling or a regional isostatic impact, incision could be maintained and dispersed across the region through continued basin growth in the wake of the transient continental divide.

Some studies suggest that as the eruptive center of the Yellowstone Hotspot migrated across southern Idaho it pushed the continental divide to the East (Pierce and Morgan, 1992; Beranek et al., 2006). However, Wegmann et al. (2007) showed that the current Yellowstone Hotspot swell does not impose a topographic signal much beyond the flanks of the Snake River Plain. Therefore, we suggest that a west to east transient uplift signal caused by plume-lithosphere interactions (delamination or mantle upwelling) was responsible for pushing the continental divide to the east. A surface erosion response should lag 1-2 m.y. behind rock-uplift caused by dynamic mantle processes as drainage capture on the leeward side of the divide works to keep up with the rate of plate motion driving the transient topographic swell (Wegmann et al., 2007). Basins on the west side of the divide continued to grow and so did the erosive power of their streams, maintaining increased incision rates.

Beranek et al (2006) used detrital zircon provenance to suggest the Twin Falls eruptive center over-printed the continental divide at ~9 Ma, at which point the divide started migrating East. However, the exact location of the divide 300km to the north, in our study area, at 9 Ma is not well constrained by the provenance data. If we assume the NW-SE orientation of the modern continental divide at these latitudes existed in the past, and was perpendicular to plate motion, then the paleo-drainage divide would have been near our study area at 9 Ma (figure 14). With continued plate

motion over the Yellowstone plume the Salmon River basin would have grown at a rate proportional to plate velocities of roughly 50 km/m.y.

Another significant factor could have been the integration of Lake Idaho into the Snake (6.4-1.7 Ma). It would be remiss to discount the potential for the Snake to drive regional incision following the eventual drainage capture of such a large drainage area, even though the initiation of incision preceded the timing of capture. Therefore, we suggest a combination of mechanisms, largely driven by the Yellowstone plume, is responsible for increased incision since 8-10 Ma, initially through uplift facilitated by lithospheric delamination as the plume is overridden by the North American Plate and then maintained by basin growth in the wake of the transient drainage divide.

5.3 CAVEATS

We focused our analysis on Fall, Carey, and Pony Creek as they provide straightforward examples of transient fluvial bedrock erosion working through the landscape. We ignored the modeling results along the South Fork and French Creek because there is clear evidence of other processes controlling the shape of the profile (i.e. glaciation and landslides). For example, the steep section on French Creek nearest the outlet occurs immediately adjacent to a topographic feature consistent with a landslide. Follow up fieldwork confirmed that a recent (Late Quaternary) landslide dammed French Creek and generated a transient lake upstream. This is evidenced by a scarp face and aggrading hillslope that impedes the path of the river. Large-scale landslides have been shown to complicate bedrock

river incision models and greatly affect the transient river profile form (Ouimet et al., 2007). Additionally, we cannot discount the possibility of glacial activity influencing the profile. For these reasons, we are skeptical of the river profile modeling approach to French Creek.

Similarly, the South Fork presents limitations to the modeling approach. Specifically, significant glaciation in its headwaters influenced both the shape of the profile and the sediment supply. The knickpoint is at a similar elevation as our other locations, but the calibrated erodibility (K) is significantly different. The South Fork drains a basin that is two orders of magnitude larger than the other tributaries, which may point to other mechanisms of fluvial erosion beyond our simple detachment-limited approach.

5.4 JUSTIFYING A DETACHMENT-LIMITED MODEL

By focusing on the simple tributary systems, we can justify the use of a detachment-limited model. Detachment-limited erosion models incise bedrock at a rate determined by the river's ability to erode the bed via abrasion or plucking (Whipple and Tucker, 2002). Erosion along Fall, Carey, and Pony Creek can be accurately described with a detachment-limited model for four reasons: (1) the tight vertical distribution in elevation of knickpoints, and (2) an $n \sim 2/3$ which is consistent with a shear stress model of bedrock incision (Howard and Kerby, 1983), (3) these creeks have very steep gradients and alluvial cover of the riverbeds is thin and easily mobilized, and (4) the model's ability to accurately reproduce the modern profile.

This detachment-limited behavior of these transient tributary systems has provided an opportunity to refine the incision history of the Salmon River between the South Fork and Riggins, Idaho. These findings have allowed us to infer the driving mechanism behind late Cenozoic regional topographic evolution of the Inland Northwest.

CHAPTER 6: CONCLUSION

The Salmon River increased its rate of incision by ~3-fold beginning ~8-10 Ma. This conclusion is based on the results from a 1D numerical model calibrated from cosmogenic erosion rates and topographic analysis of eleven tributary basins. The cosmogenic erosion rates we present are in agreement with other studies on the local and regional scale. Erosion rates increase 2.4-fold while channel steepness indices increase 3.8-fold as the landscape adjusts to the wave of incision. This relationship validates our use of a detachment-limited model that quantifies erosion through shear stress on the riverbed. Our date of 8-10 Ma is similar to other studies within the Idaho Batholith and central Idaho. This agreement suggests that the region responded as a whole to a change in baselevel.

We hypothesize that the initial pulse of incision was in response to surface-uplift resulting from lithospheric delamination facilitated by the Yellowstone plume. Our model shows that the pulse of incision has been persistent since 8-10 Ma. We propose that incision was maintained by down-cutting along the Salmon River, which was driven by continued basin growth on the east side of the transient continental divide and the eventual integration of the Snake River Plain into the Snake River. The combination of these mechanisms drove a surface response that increased canyon relief by an average of one kilometer. We favor this interpretation based on the timing of a southward spreading plume head as it impacted the base of the North American craton, evidence of delamination in recent tomographic images, and a northward trend in decreasing incision rates away from the focal center of delamination. In conclusion, mantle plume-lithosphere interactions are largely

responsible for the deeply incised canyons and the dynamic, transient landscape across the Inland Northwest.

REFERENCES

- Anderson, Alfred L. "Cretaceous and Tertiary planation in northern Idaho." *The Journal of Geology* (1929): 747-764.
- Barry, T. L., S. Self, S. P. Kelley, S. Reidel, P. Hooper, and M. Widdowson. "New $^{40}\text{Ar}/^{39}\text{Ar}$ dating of the Grande Ronde lavas, Columbia River Basalts, USA: implications for duration of flood basalt eruption episodes." *Lithos* 118, no. 3 (2010): 213-222.
- Barry, T. L., S. P. Kelley, S. P. Reidel, V. E. Camp, S. Self, N. A. Jarboe, R. A. Duncan, and P. R. Renne. "Eruption chronology of the Columbia River Basalt Group." *Geological Society of America Special Papers* 497 (2013): 45-66.
- Beranek, Luke P., Paul Karl Link, and C. Mark Fanning. "Miocene to Holocene landscape evolution of the western Snake River Plain region, Idaho: Using the SHRIMP detrital zircon provenance record to track eastward migration of the Yellowstone hotspot." *Geological Society of America Bulletin* 118, no. 9-10 (2006): 1027-1050.
- Bierman, Paul, and ERIC J. Steig. "Estimating rates of denudation using cosmogenic isotope abundances in sediment." *Earth surface processes and landforms* 21, no. 2 (1996): 125-139.
- Blackwelder, Eliot. "The Old Erosion Surface in Idaho: A Criticism." *The Journal of Geology* (1912): 410-414.

- Bonnichsen, Bill. "The Bruneau-Jarbridge eruptive center, southwestern Idaho." *Cenozoic Geology of Idaho: Idaho Bureau of Mines and Geology Bulletin 26* (1982): 237-254.
- Brown, Erik Thorson, Robert F. Stallard, Matthew C. Larsen, Grant M. Raisbeck, and Françoise Yiou. "Denudation rates determined from the accumulation of in situ-produced ^{10}Be in the Luquillo Experimental Forest, Puerto Rico." *Earth and Planetary Science Letters* 129, no. 1 (1995): 193-202.
- Burov, Evgene, Laurent Guillou-Frottier, Elia d'Acremont, Latetia Le Pourhiet, and S. A. P. L. Cloetingh. "Plume head–lithosphere interactions near intra- continental plate boundaries." *Tectonophysics* 434, no. 1 (2007): 15-38.
- Camp, Victor E. "Geological Society of America Special Papers." (2013).
- Camp, Victor E., and Martin E. Ross. "Mantle dynamics and genesis of mafic magmatism in the intermontane Pacific Northwest." *Journal of Geophysical Research: Solid Earth (1978–2012)* 109, no. B8 (2004).
- Chmeleff, Jerome, Friedhelm von Blanckenburg, Karsten Kossert, and Dieter Jakob. "Determination of the ^{10}Be half-life by Multi Collector ICP-mass spectrometry and liquid scintillation counting." *Geochimica et Cosmochimica Acta Supplement 73* (2009): 221.
- Clark, Marin K., Gweltaz Maheo, Jason Saleeby, and Kenneth A. Farley. "The non-equilibrium landscape of the southern Sierra Nevada, California." *GSA TODAY* 15, no. 9 (2005): 4.

- Crough, S. Thomas. "Thermal origin of mid-plate hot-spot swells." *Geophysical Journal International* 55, no. 2 (1978): 451-469.
- Davies, Geoffrey F. "Topography: a robust constraint on mantle fluxes." *Chemical geology* 145, no. 3 (1998): 479-489.
- Ferrier, Ken L., James W. Kirchner, and Robert C. Finkel. "Estimating millennial-scale rates of dust incorporation into eroding hillslope regolith using cosmogenic nuclides and immobile weathering tracers." *Journal of Geophysical Research: Earth Surface (2003–2012)* 116, no. F3 (2011).
- Flint, J.J., Stream gradient as a function of order, magnitude, and discharge, *Water Resour. Res.*, 10(1974): 969-973.
- Gilbert, Grove Karl. "The convexity of hilltops." *The Journal of Geology* 17, no. 4 (1909): 344-350.
- Gosse, John C., and Fred M. Phillips. "Terrestrial in situ cosmogenic nuclides: theory and application." *Quaternary Science Reviews* 20, no. 14 (2001): 1475-1560.
- Granger, Darryl E., James W. Kirchner, and Robert Finkel. "Spatially averaged long-term erosion rates measured from in situ-produced cosmogenic nuclides in alluvial sediment." *The Journal of Geology* (1996): 249-257.
- Hack, John Tilton. *Interpretation of erosional topography in humid temperate regions*. Bobbs-Merrill, 1960.

Hack, JOHN T. "Stream-profile analysis and stream-gradient index." *Journal of Research of the US Geological Survey* 1, no. 4 (1973): 421-429.

Hidy, Alan. "Cosmogenic Nuclide Quantification of Paleo-fluvial Sedimentation Rates in Response to Climate Change." PhD diss., 2013.

Howard, Alan D., and Gordon Kerby. "Channel changes in badlands." *Geological Society of America Bulletin* 94, no. 6 (1983): 739-752.

Izett, Glen A. "Volcanic ash beds: Recorders of upper Cenozoic silicic pyroclastic volcanism in the western United States." *Journal of Geophysical Research: Solid Earth (1978–2012)* 86, no. B11 (1981): 10200-10222.

Jeffery, M. Louise, Todd A. Ehlers, Brian J. Yanites, and Christopher J. Poulsen. "Quantifying the role of paleoclimate and Andean Plateau uplift on river incision." *Journal of Geophysical Research: Earth Surface* 118, no. 2 (2013): 852-871.

Jordan, Brennan T., Anita L. Grunder, Robert A. Duncan, and Alan L. Deino. "Geochronology of age-progressive volcanism of the Oregon High Lava Plains: Implications for the plume interpretation of Yellowstone." *Journal of Geophysical Research: Solid Earth (1978–2012)* 109, no. B10 (2004).

Kirchner, James W., Robert C. Finkel, Clifford S. Riebe, Darryl E. Granger, James L. Clayton, John G. King, and Walter F. Megahan. "Mountain erosion over 10 yr, 10 ky, and 10 my time scales." *Geology* 29, no. 7 (2001): 591-594.

Lal, D. "Cosmic ray labeling of erosion surfaces: in situ nuclide production rates and erosion models." *Earth and Planetary Science Letters* 104, no. 2 (1991): 424-439.

Link, Paul K., and Mary KV Hodges. "The Neogene drainage history of south-central Idaho." *Field Guides* 21 (2011): 103-123.

Lund, Karen, Lawrence W. Snee, and Karl V. Evans. "Age and genesis of precious metals deposits, Buffalo Hump District, central Idaho; implications for depth of emplacement of quartz veins." *Economic Geology* 81, no. 4 (1986): 990- 996.

Meyer, Grant A., and Matt E. Leidecker. "Fluvial terraces along the Middle Fork Salmon River, Idaho, and their relation to glaciation, landslide dams, and incision rates: A preliminary analysis and river-mile guide." *Guidebook to the Geology of Eastern Idaho. Pocatello (ID): Idaho Museum of Natural History* (1999): 219-235.

Morgan, W. Jason. "Deep mantle convection plumes and plate motions." *AAPG Bulletin* 56, no. 2 (1972): 203-213.

Neville, Colleen, NEIL D. Opdyke, EVERETT H. Lindsay, and NOYE M. Johnson. "Magnetic stratigraphy of Pliocene deposits of the Glens Ferry Formation, Idaho, and its implications for North American mammalian biostratigraphy." *American Journal of Science* 279, no. 5 (1979): 503-526.

Niemann, Jeffrey D., Nicole M. Gasparini, Gregory E. Tucker, and Rafael L. Bras.

"A quantitative evaluation of Playfair's law and its use in testing long-term stream erosion models." *Earth Surface Processes and Landforms* 26, no. 12 (2001): 1317-1332.

Ouimet, William B., Kelin X. Whipple, Leigh H. Royden, Zhiming Sun, and

Zhiliang Chen. "The influence of large landslides on river incision in a transient landscape: Eastern margin of the Tibetan Plateau (Sichuan, China)." *Geological Society of America Bulletin* 119, no. 11-12 (2007): 1462-1476.

Othberg, K. L., Bill Bonnicksen, C. C. Swisher III, and M. M. Godchaux.

"Geochronology and geochemistry of Pleistocene basalts of the western Snake River Plain and Smith Prairie." *Idaho: Isochron/West* 62 (1995): 16- 29.

Perkins, Michael E., Francis H. Brown, William P. Nash, S. K. Williams, and

William McIntosh. "Sequence, age, and source of silicic fallout tuffs in middle to late Miocene basins of the northern Basin and Range province." *Geological Society of America Bulletin* 110, no. 3 (1998): 344-360.

Pierce, Kenneth L., and Lisa A. Morgan. "The track of the Yellowstone hot spot:

Volcanism, faulting, and uplift." *Geological Society of America Memoirs* 179 (1992): 1-54.

Ross, Clyde P. "Mesozoic and Tertiary granitic rocks in Idaho." *The Journal of*

Geology (1928): 673-693.

Reidel, Stephen P., Victor E. Camp, Terry L. Tolan, and Barton S. Martin. "The Columbia River flood basalt province: Stratigraphy, areal extent, volume, and physical volcanology." *Geological Society of America Special Papers* 497 (2013): 1-43.

Schildgen, T. F., W. M. Phillips, and R. S. Purves. "Simulation of snow shielding corrections for cosmogenic nuclide surface exposure studies." *Geomorphology* 64, no. 1 (2005): 67-85.

Schofield, S. "J.(1915): Geology of Cranbrook Area." *Geol. Surv., Canada, Mem* 76: 245.

Shervais, John W., and Barry B. Hanan. "Lithospheric topography, tilted plumes, and the track of the Snake River–Yellowstone hot spot." *Tectonics* 27, no. 5 (2008).

Smith, Gerald R., Neil Morgan, and Eric Gustafson. "Fishes of the Mio-Pliocene Ringold Formation, Washington: pliocene capture of the snake river by the Columbia River." (2000).

Smith, Robert B., Michael Jordan, Bernhard Steinberger, Christine M. Puskas, Jamie Farrell, Gregory P. Waite, Stephan Husen, Wu-Lung Chang, and Richard O'Connell. "Geodynamics of the Yellowstone hotspot and mantle plume: Seismic and GPS imaging, kinematics, and mantle flow." *Journal of Volcanology and Geothermal Research* 188, no. 1 (2009): 26-56.

- Sweetkind, Donald S., and David D. Blackwell. "Fission-track evidence of the Cenozoic thermal history of the Idaho batholith." *Tectonophysics* 157, no. 4 (1989): 241-250.
- Tucker, Gregory E., and Rudy Slingerland. "Drainage basin responses to climate change." *Water Resources Research* 33, no. 8 (1997): 2031-2047.
- Umpleby, Joseph B. "An old erosion surface in Idaho: its age and value as a datum plane." *The Journal of Geology* (1912): 139-147.
- Usgs dem
- Valera, J. L., A. M. Negrodo, and Ivone Jiménez-Munt. "Deep and near-surface consequences of root removal by asymmetric continental delamination." *Tectonophysics* 502, no. 1 (2011): 257-265.
- Van Tassell, Jay, M. Ferns, V. McConnell, and G. R. Smith. "The mid-Pliocene Imbler fish fossils." *Grande Ronde Valley, Union County, Oregon, and the connection between Lake Idaho and the Columbia River: Oregon Geology* 63, no. 3 (2001): 77-84.
- Vogl, James J., Kyoungwon Min, Alberto Carmenate, David A. Foster, and Antonios Marsellos. "Miocene regional hotspot-related uplift, exhumation, and extension north of the Snake River Plain: Evidence from apatite (U- Th)/He thermochronology." *Lithosphere* 6, no. 2 (2014): 108-123.
- Wegmann, Karl W., Brian D. Zurek, Christine A. Regalla, Dario Bilardello, Jennifer L. Wollenberg, Sarah E. Kopczynski, Joseph M. Ziemann et al.

"Position of the Snake River watershed divide as an indicator of geodynamic processes in the greater Yellowstone region, western North America."

Geosphere 3, no. 4 (2007): 272-281.

Whipple, Kelin X., and Gregory E. Tucker. "Dynamics of the stream-power river incision model: Implications for height limits of mountain ranges, landscape response timescales, and research needs." *Journal of Geophysical Research: Solid Earth (1978–2012)* 104, no. B8 (1999): 17661-17674.

Whipple, Kelin X., and Gregory E. Tucker. "Implications of sediment-flux-dependent river incision models for landscape evolution." *Journal of Geophysical Research: Solid Earth (1978–2012)* 107, no. B2 (2002): ETG-3.

Willett, Sean D., Scott W. McCoy, J. Taylor Perron, Liran Goren, and Chia-Yu Chen. "Dynamic reorganization of river basins." *Science* 343, no. 6175 (2014): 1248765.

Wobus, Cameron, Kelin X. Whipple, Eric Kirby, Noah Snyder, Joel Johnson, Katerina Spyropolou, Benjamin Crosby, and Daniel Sheehan. "Tectonics from topography: Procedures, promise, and pitfalls." *Geological Society of America Special Papers* 398 (2006): 55-74.

Wood, Spencer H., and Drew M. Clemens. "Geologic and tectonic history of the western Snake River Plain, Idaho and Oregon." *Tectonic and Magmatic Evolution of the Snake River Plain Volcanic Province: Idaho Geological Survey Bulletin* 30 (2002): 69-103.

Yanites, Brian J., Todd A. Ehlers, Jens K. Becker, Michael Schnellmann, and Stefan Heuberger. "High magnitude and rapid incision from river capture: Rhine River, Switzerland." *Journal of Geophysical Research: Earth Surface* 118, no. 2 (2013): 1060-1084.

Yuan, Huaiyu, and Ken Dueker. "Teleseismic P-wave tomogram of the Yellowstone plume." *Geophysical Research Letters* 32, no. 7 (2005).

TABLES

TABLE 1: BASIN CHARACTERISTICS

| | basin | Lat | Long | drainage area (m ²) | ¹⁰ Be (atoms/g) | production rate (atoms/yr) | E (mm/yr) | mean slope (°) | knickpoint elevation (m) | % of basin that is relict | snow corrected E | % drop in E | relict k_{sn} | adjusted k_{sn} |
|-----------|-------------|--------|---------|---------------------------------|----------------------------|----------------------------|--------------|----------------|--------------------------|---------------------------|------------------|-------------|-----------------|-------------------|
| relict | Upper Fall | 45.373 | 116.011 | 10E+06 | 29.2E+04 | 27.97 | 0.064 ± .007 | 14 | na | 100 | 0.049 ± .007 | 23 | 115 | na |
| basins | Burgdorf | 45.271 | 115.908 | 84E+04 | 38.8E+04 | 26.68 | 0.046 ± .005 | 13 | na | 100 | 0.035 ± .005 | 22 | 35 | na |
| | Chinook | 45.226 | 115.804 | 04E+06 | 21.6E+04 | 26.70 | 0.082 ± .01 | 16 | na | 100 | 0.063 ± .01 | 23 | 55 | na |
| | Seceah Rd | 45.255 | 115.814 | 05E+06 | 25.0E+04 | 26.79 | 0.071 ± .008 | 15 | na | 100 | 0.055 ± .008 | 23 | 45 | na |
| adjusted | Longtom | 45.459 | 115.881 | 08E+06 | 09.1E+04 | 19.66 | 0.15 ± .019 | 26 | na | 0 | 0.14 ± .019 | 6 | na | 300 |
| basins | Tailholt* | 45.043 | 115.677 | 05E+06 | 12.2E+04 | 22.23 | 0.12 ± .015 | 24 | na | 0 | 0.11 ± .015 | 9 | na | 210 |
| | Circle End* | 45.047 | 115.667 | 03E+06 | 13.0E+04 | 21.08 | 0.11 ± .014 | 25 | na | 0 | 0.1 ± .014 | 8 | na | 210 |
| transient | Fall | 45.432 | 115.983 | 44E+06 | 21.5E+04 | 23.27 | 0.073 ± .009 | 18 | 1746 | 32 | 0.063 ± .009 | 13 | 115 | 410 |
| basins | Carey | 45.452 | 115.949 | 17E+06 | 21.7E+04 | 24.47 | 0.076 ± .009 | 22 | 1888 | 25 | 0.065 ± .009 | 14 | 105 | 360 |
| | Pony | 45.188 | 115.573 | 32E+06 | 14.8E+04 | 27.31 | 0.12 ± .014 | 19 | 1865 | 27 | 0.1 ± .014 | 17 | 90 | 310 |
| | South Fork# | 45.175 | 115.581 | 21E+08 | 11.3E+04 | 28.33 | 0.17 ± .018 | 18 | 1704 | 84 | 0.13 ± .018 | 23 | 60 | 230 |
| | French# | 45.421 | 116.027 | 01E+08 | 15.5E+04 | 26.39 | 0.11 ± .014 | 16 | 1211 | 62 | 0.092 ± .014 | 19 | 170 | 440 |

na- not applicable
*data from Kirchner et al., 2001
#basins that show signs of significant glaciation or recent landslides

TABLE 2: SIX DIFFERENT PARAMETER SETS

| | rock-uplift rate (mm/yr) | K | m | n |
|---|-----------------------------|----------|-------|------|
| 1 | 0.035 | 1.94E-06 | 0.307 | 0.66 |
| 2 | 0.05 | 2.76E-06 | 0.307 | 0.66 |
| 3 | 0.063 | 3.52E-06 | 0.307 | 0.66 |
| 4 | 0.035 | 4.37E-07 | 0.465 | 1 |
| 5 | 0.05 | 6.25E-07 | 0.465 | 1 |
| 6 | 0.063 | 7.92E-07 | 0.465 | 1 |

FIGURES

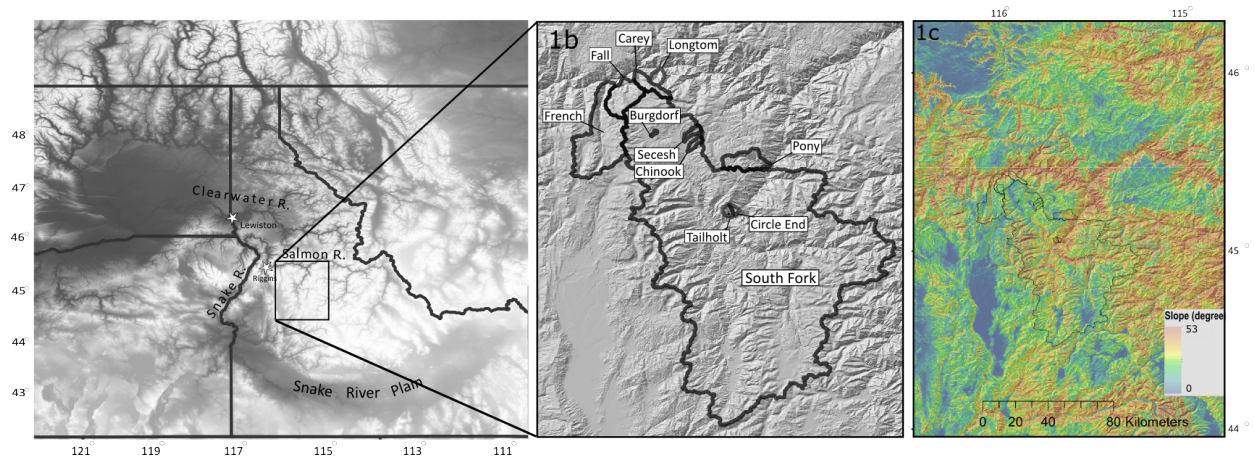


Figure 1: Study Area. [a] The Inland Northwest. [b] Zoomed in view of the eleven tributaries of the Salmon River. [c] A slope map of the study area showing extent of incision. The headward advance of the transient signal is marked by the transition from steep slopes (red) to gentle slopes (blue).

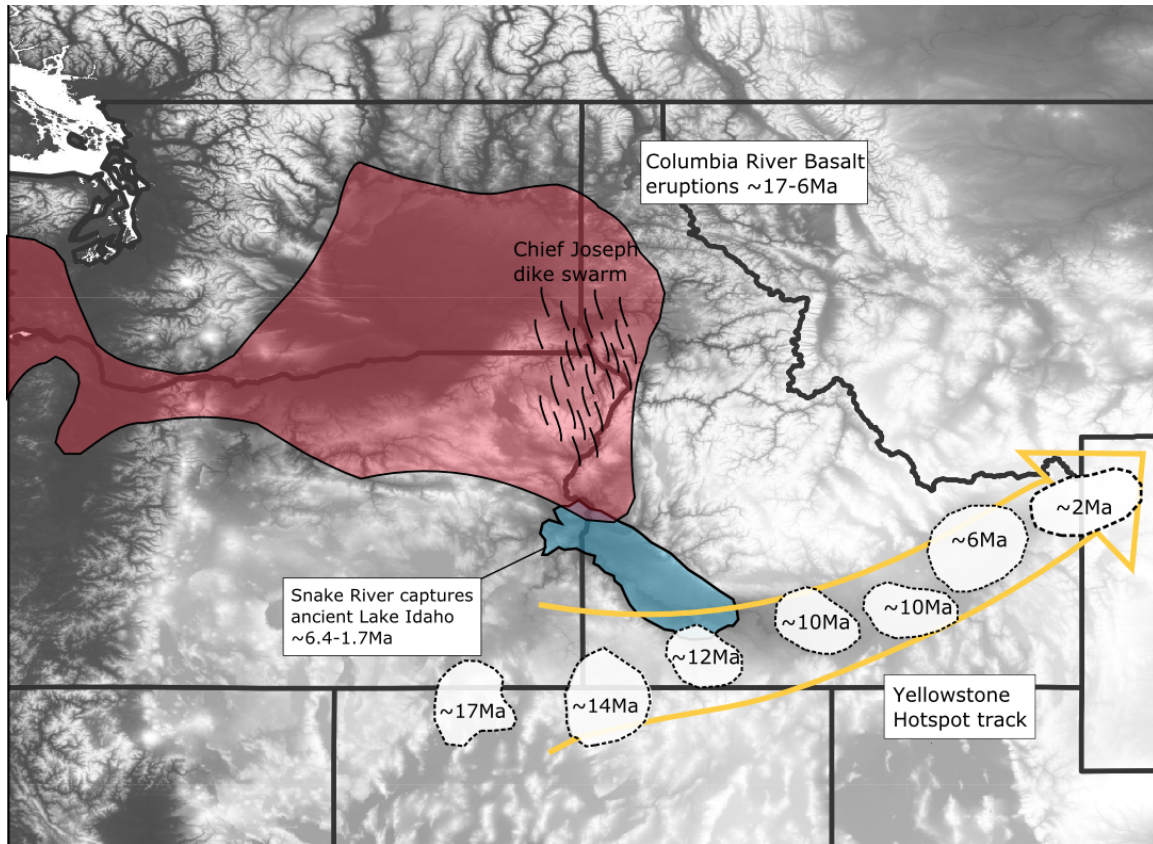


Figure 2: Major geologic events of the late Cenozoic that could have affected regional baselevel change. The areal extent of Columbia River Basalt emplacement is shaded in red. The areal extent of Lake Idaho is shaded in blue. The path of the Yellowstone Hotspot-track is marked by the time-transgression of eruptive centers along the yellow arrow.

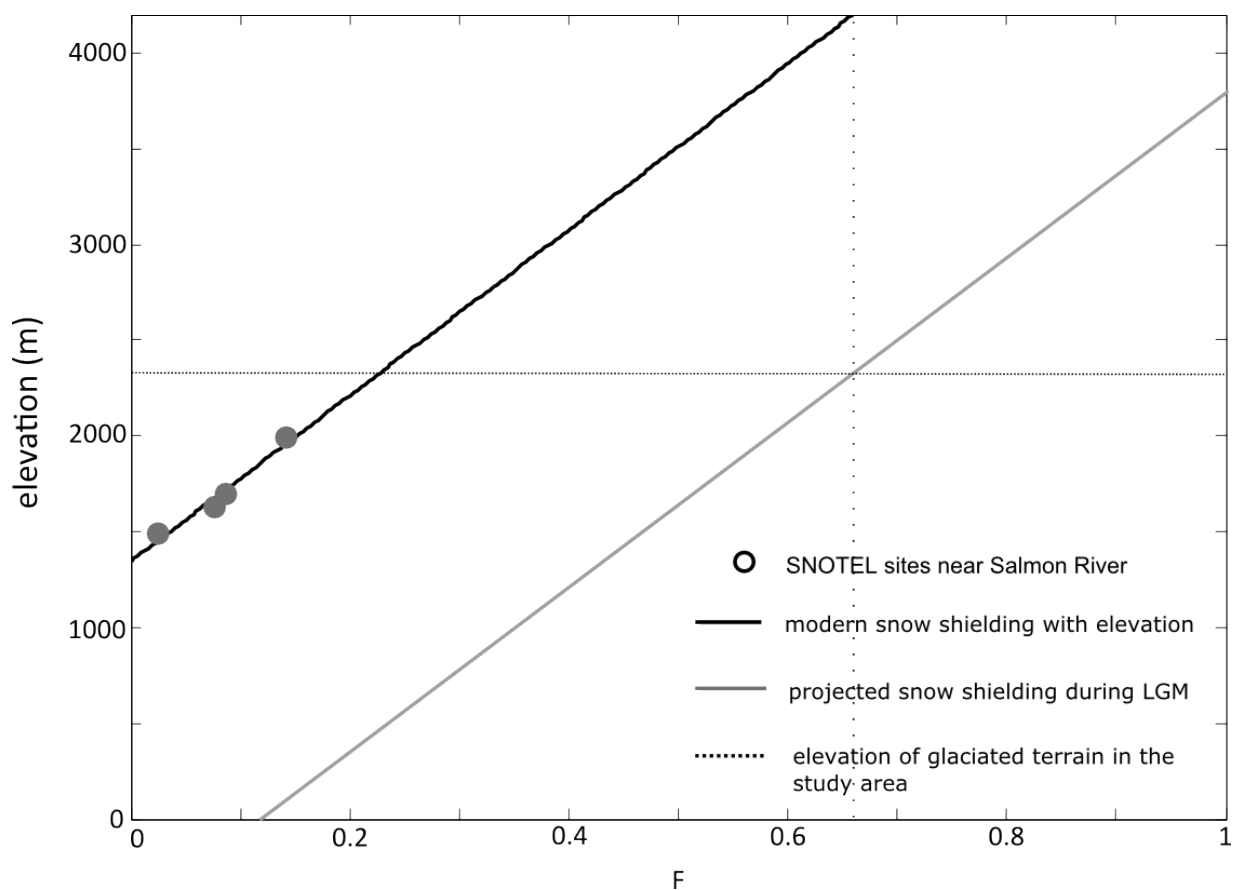


Figure 3: Snow cover corrections. Data from four SNOTEL sites: Bear Basin, Secesh Summit, Long Valley, and West Branch. F is the fraction of total cosmic rays attenuated by snow calculated from the yearly average water equivalency data from 1981 to 2014 at each site. Projected attenuation by snow during LGM is estimated by shifting the regression to line up the minimum elevation of observed glaciated topography in the headwaters of the South Fork basin with $2/3$ attenuation by snow cover.

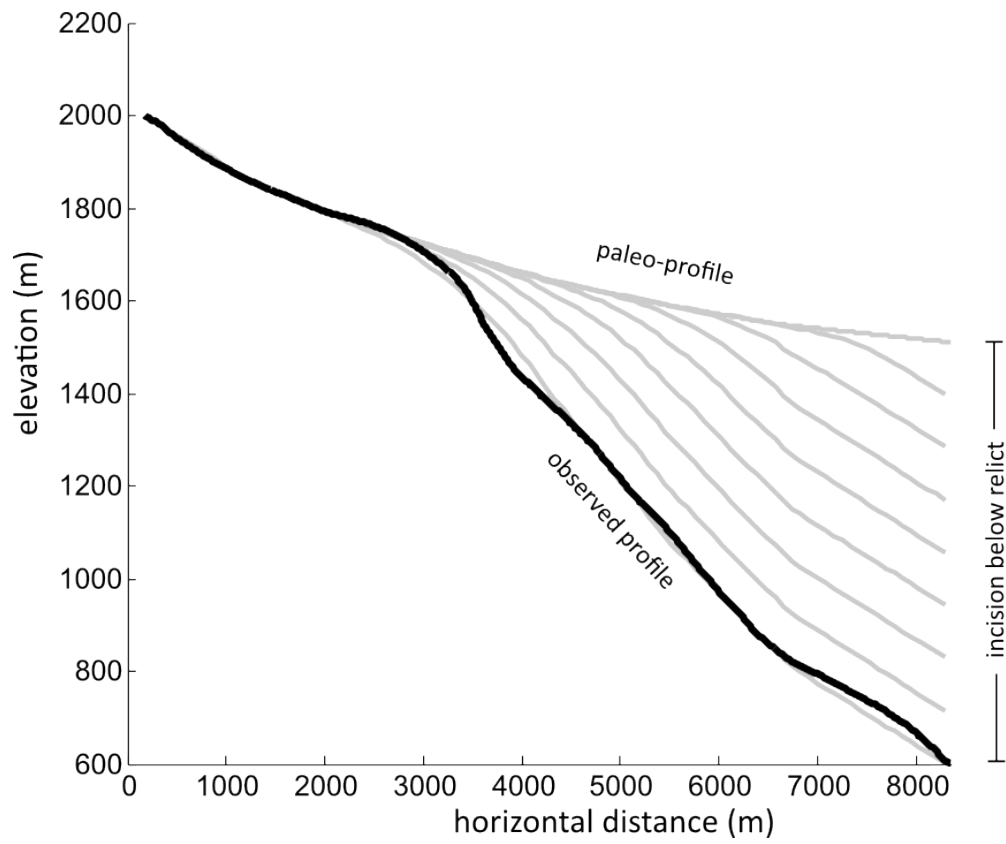


Figure 4: Example model run. The evolution of the paleo-profile through time as the mouth of the tributary is lowered to its modern position.

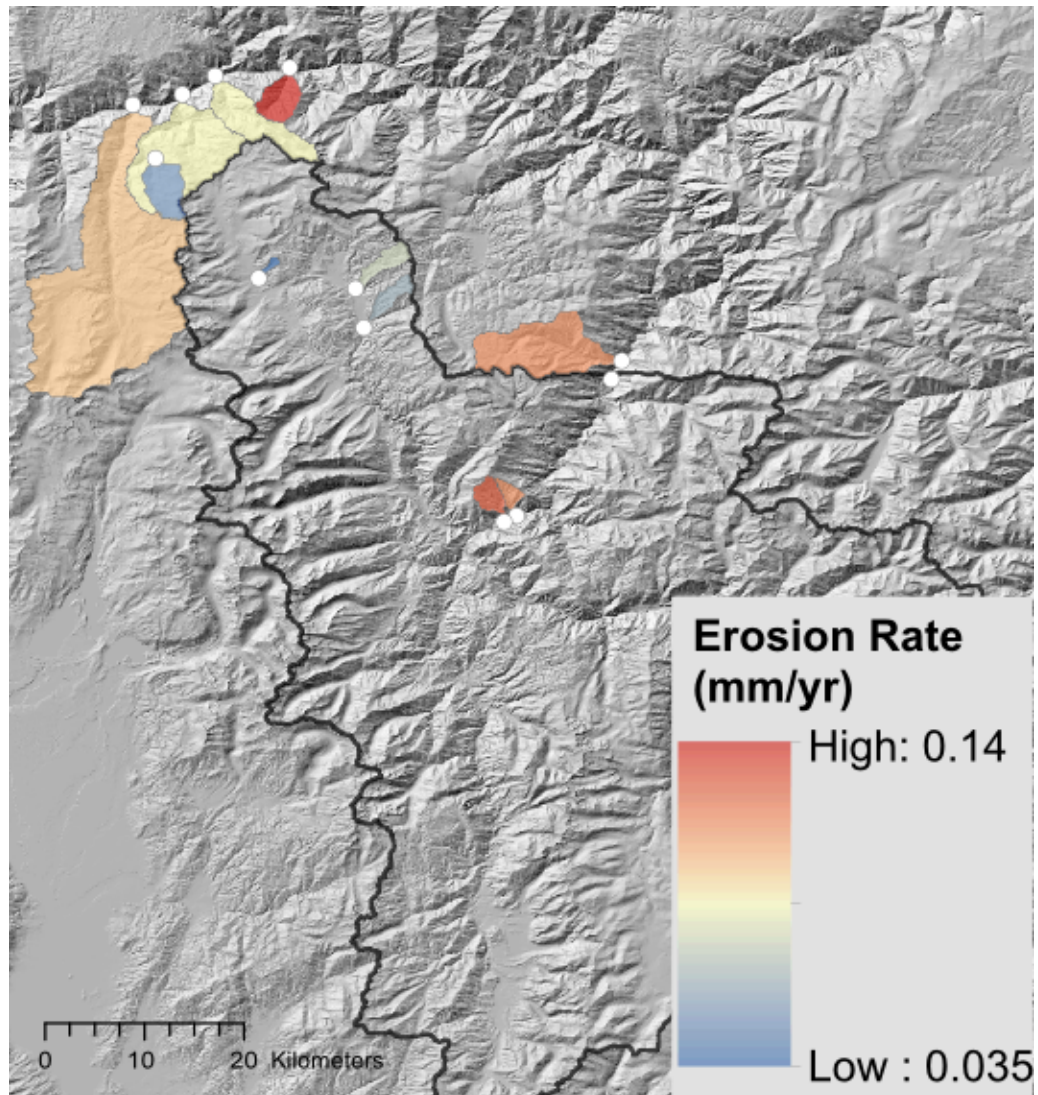


Figure 6: Basin averaged erosion rates. White circles are sample locations. Erosion rates range from 0.035 mm/yr to 0.14 mm/yr. The South Fork is not colored for visual purposes. Erosion rate in the South Fork is 0.13 mm/yr.

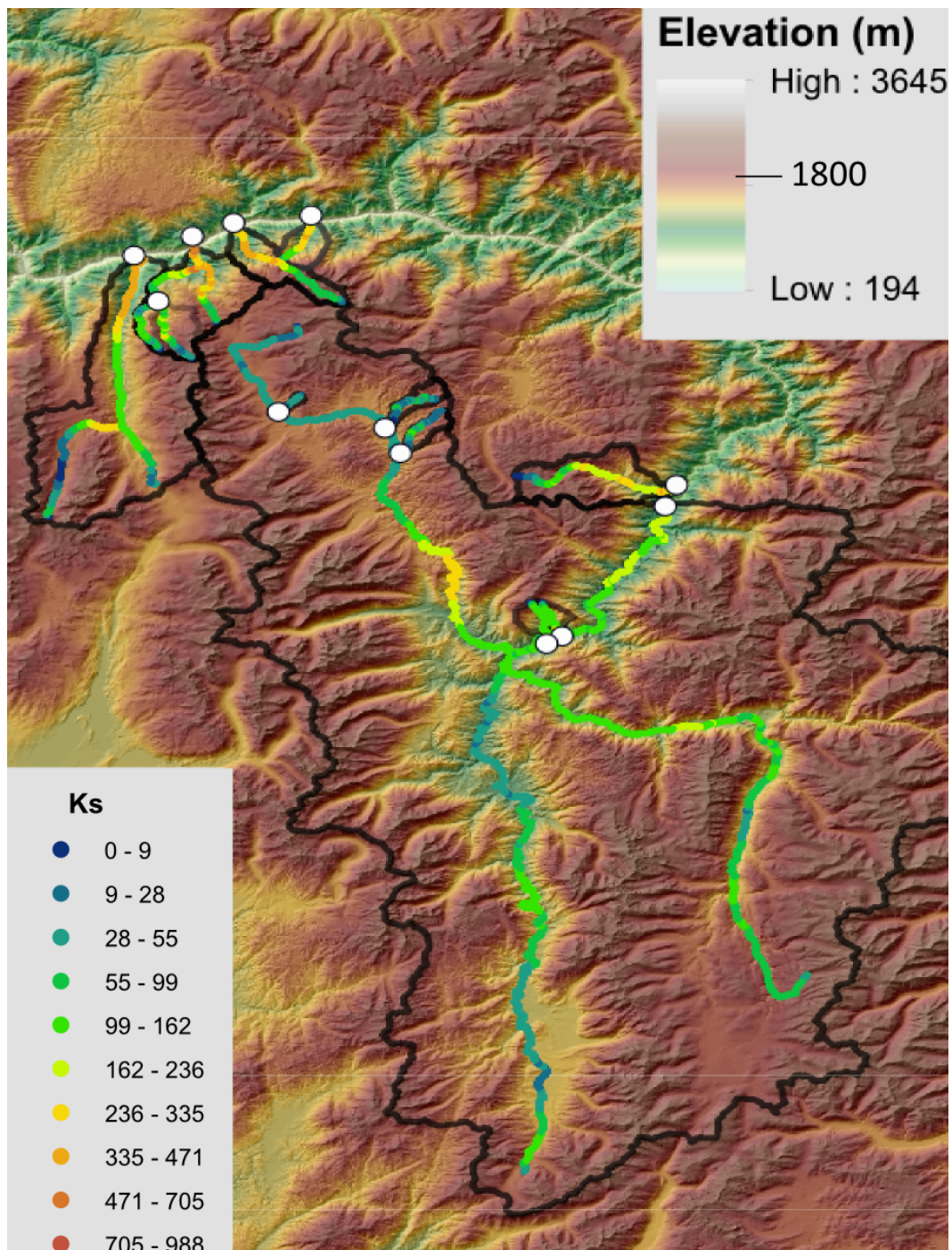


Figure 7: Steepness profiles and elevation map. White circles mark the mouth of the streams. Knickpoints occur at the transition from low to high steepness. Most knickpoints in the study area are around 1800m in elevation.

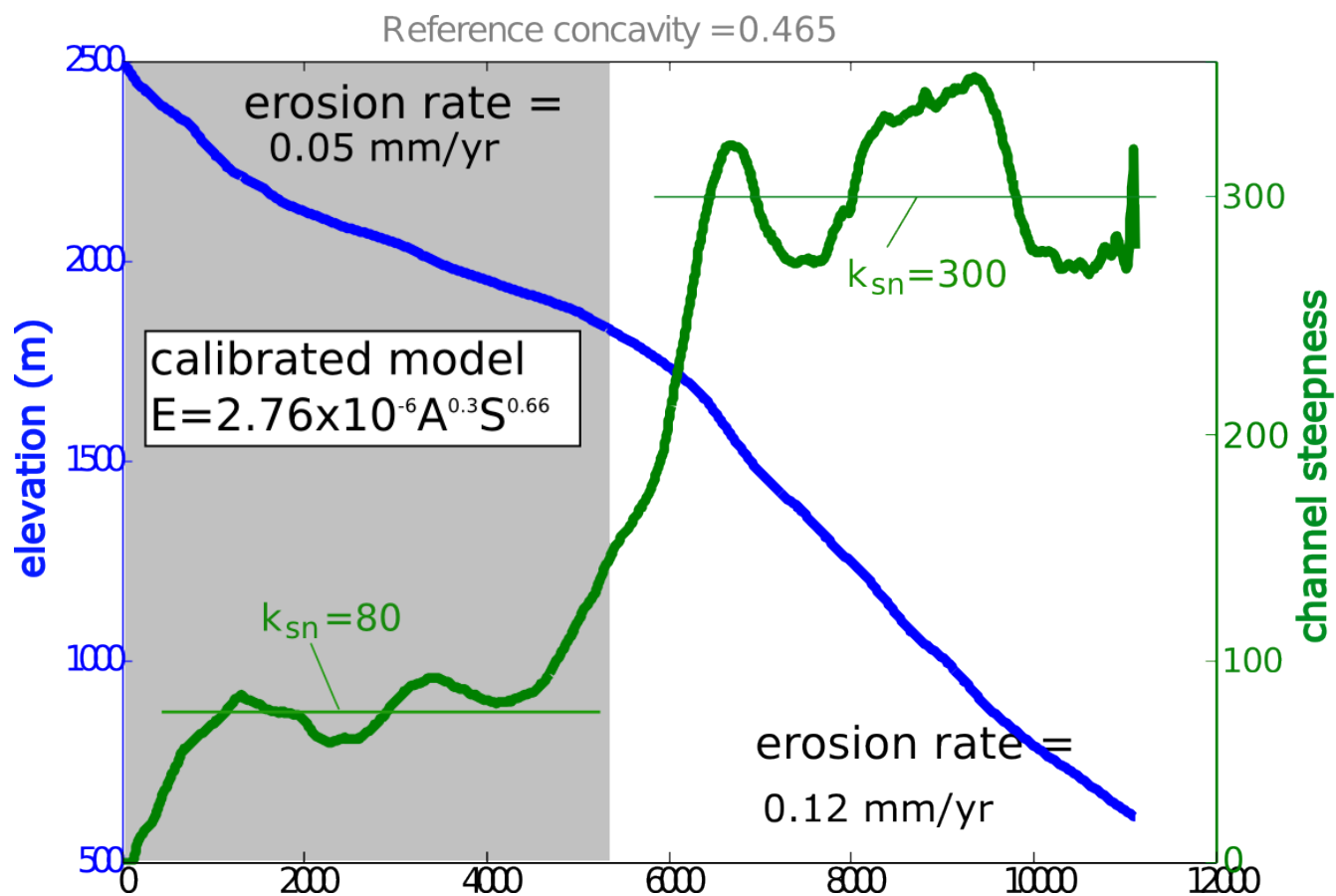


Figure 7: Model calibration. Example of a transient basin river profile, shown in blue, and normalized steepness k_{sn} shown in green. The shaded region covers the relict domain of the stream and the un-shaded region covers the adjusted domain of the stream. Erosion rate increases by a factor of 2.4 from relict to adjusted landscape. Normalized steepness increases by a factor of 3.8 from relict to adjusted landscape.

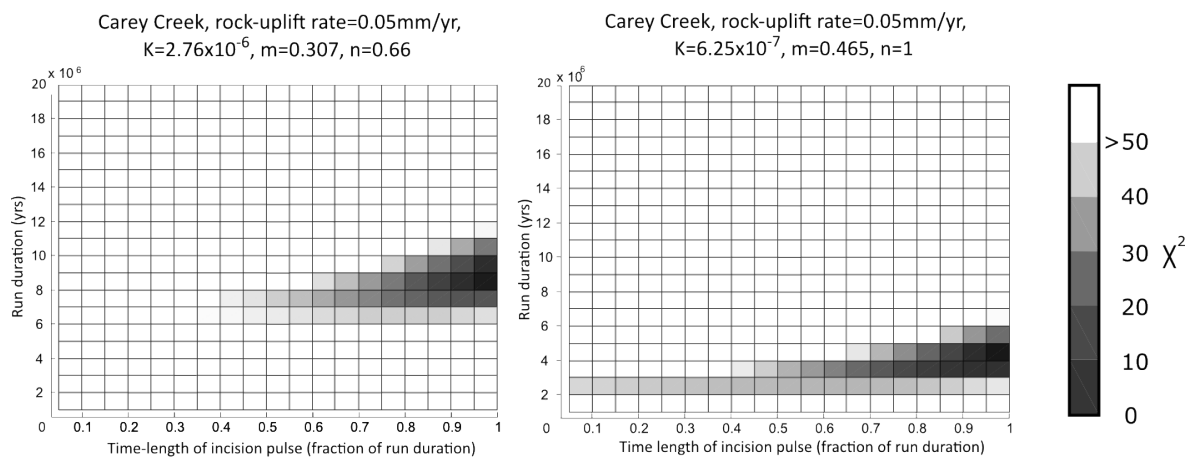


Figure 8: Example of χ^2 misfit test. Darker colors represent the smallest misfit between simulated and observed river profiles. The smallest misfits for all basins occur at pulse of accelerated incision=1 (when there is no variation in incision rate).

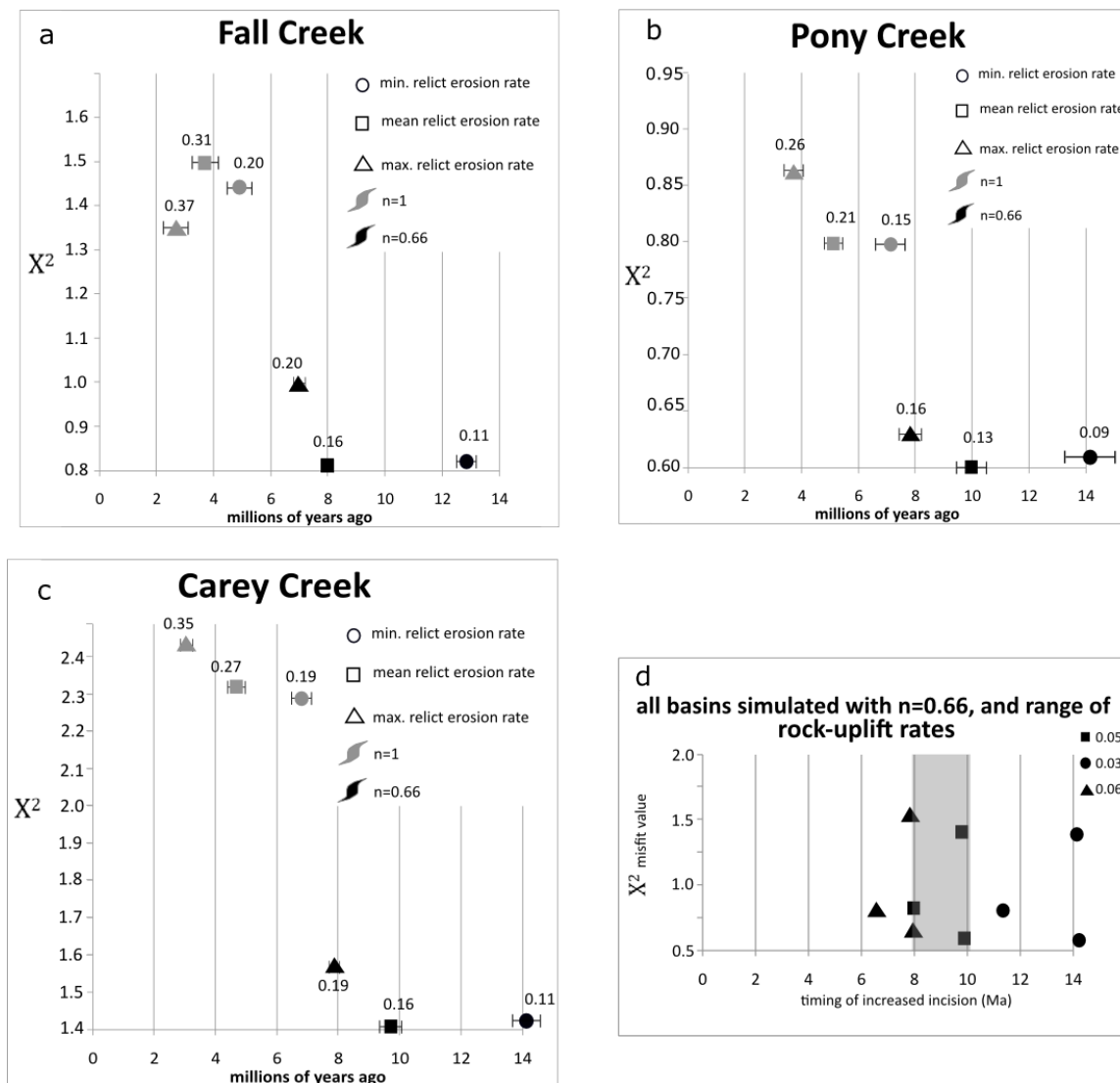


Figure 9: [A-C]: X^2 misfit results for each basin for model runs using different relict erosion rates and n . Each data point also displays the incision rate at the mouth of the tributary. Error bars show the range of timing for model runs within 25% of the lowest X^2 value. [D] is a summary A-C using a shear stress model ($n=0.66$). Using the mean relict erosion rate within the shear stress model yields a timing of 7-9 Ma for an increase in incision rate. The average increased incision rate is 0.15 mm/yr for the preferred model runs.

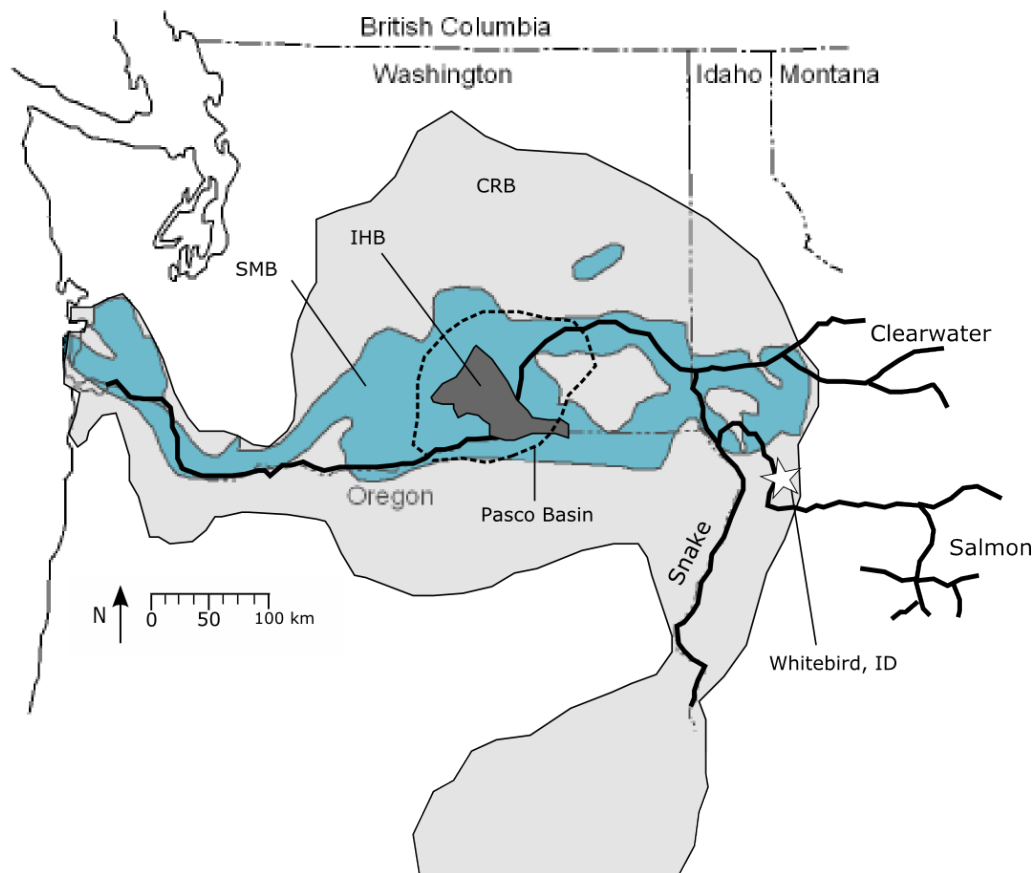


Figure 10: Map of Columbia River Basalt. Modified from Reidel et al., 2014. The Columbia River Basalts (CRB) shown in light-gray, include all subgroups of the CRB that were emplaced from 17.5-6 Ma. Lava emanating from dike swarms in S.E. Washington, N.E. Oregon, and Idaho flowed west into the Columbia River Drainage system. Sections of basalt 3.2 km thick remain in the Pasco Basin, and sections 1.2 km thick remain near Whitebird, ID. The Saddle Mountain Basalt (SMB) is shown in blue, was emplaced from 13-6 Ma. The Ice Harbor Basalt (IHB) shown in dark-gray, was emplaced 8.5 Ma.

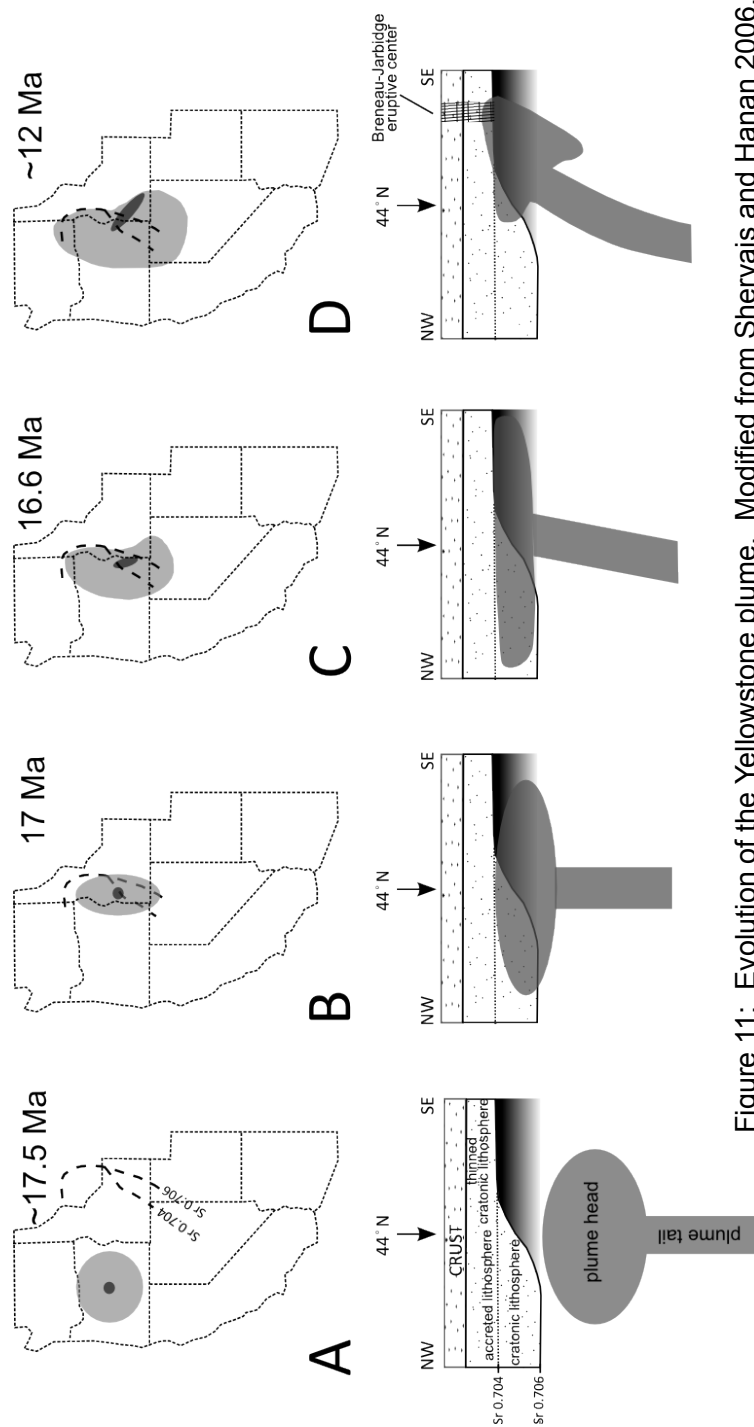


Figure 11: Evolution of the Yellowstone plume. Modified from Shervais and Hanan 2006. Sequential map view and cross sections of the model showing the rise and deformation of the plume head (light-gray) and plume tail (dark-gray) as it interacts with lithosphere of western North America; cross section view is looking east toward the cratonic lithosphere. The cross sections are 'compressed views showing lithosphere thickness under accreted terranes (dotted line) that corresponds to the Sr 0.704 line, cratonic lithosphere (pattern) that corresponds to the Sr 0.706 line, and thinned cratonic lithosphere (gradient). [A] Plume head and tail are concentric as they rise through the asthenosphere beneath east central Oregon prior to impact with lithosphere. [B] Plume head impacts and flattens against base of lithosphere to form extensive decompression melts; at the same time, the plume head is compressed to north and south as it flattens against accreted lithosphere and beneath thinned lithosphere. [C] Plume head continues to deform against the western cratonic margin; plume tail follows the head south. [D] Plume tail becomes established in thermally eroded sublithospheric channel sink, guided by preexisting zone of thin lithosphere.

Influence of flood basalts on river profile

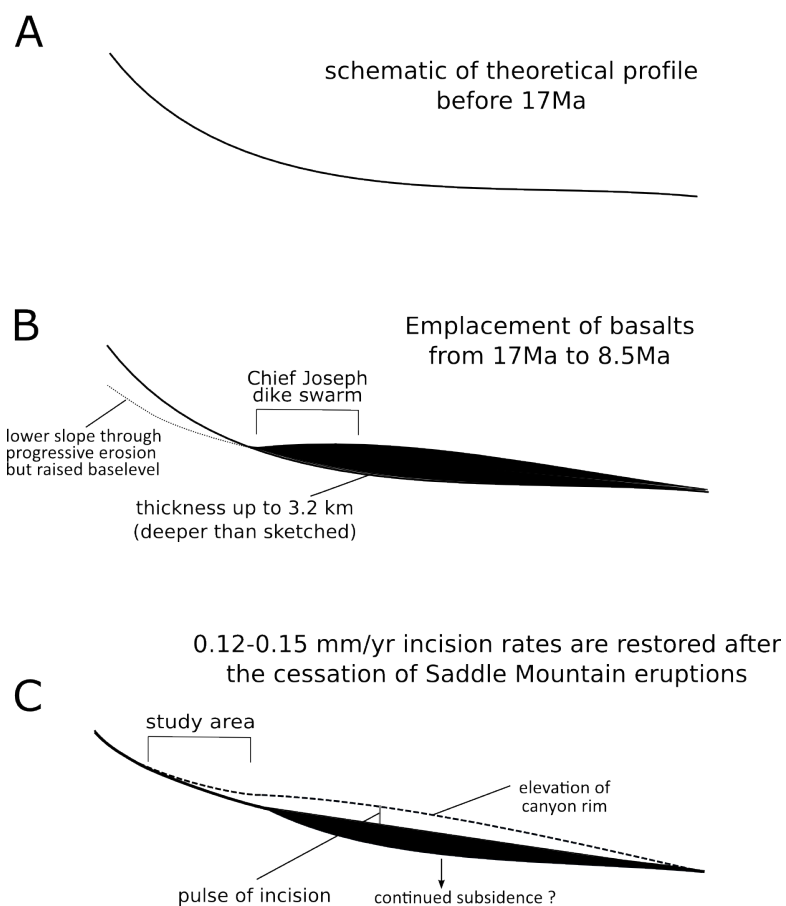


Figure 12: The influence of flood basalts on the river profile. [A] Theoretical river profile of the Columbia River network prior to CRB eruptions. The profile extends from our study area in the headwaters to the Pacific Ocean. At this time incision rates in our study area are near 0.15 mm/yr. [B] Basalts are emplaced beginning 17 Ma and the local baselevel downstream of the Chief Joseph dike swarm rises. This rise in baselevel decreases slope thereby decreasing erosion for the next 11 My. [C] After 11 My of slower erosion rates the upstream reach has developed a gentler slope. Following the cessation of CRBs baselevel lowers as incision rates are restored uninhibited by valley filling flood basalts.

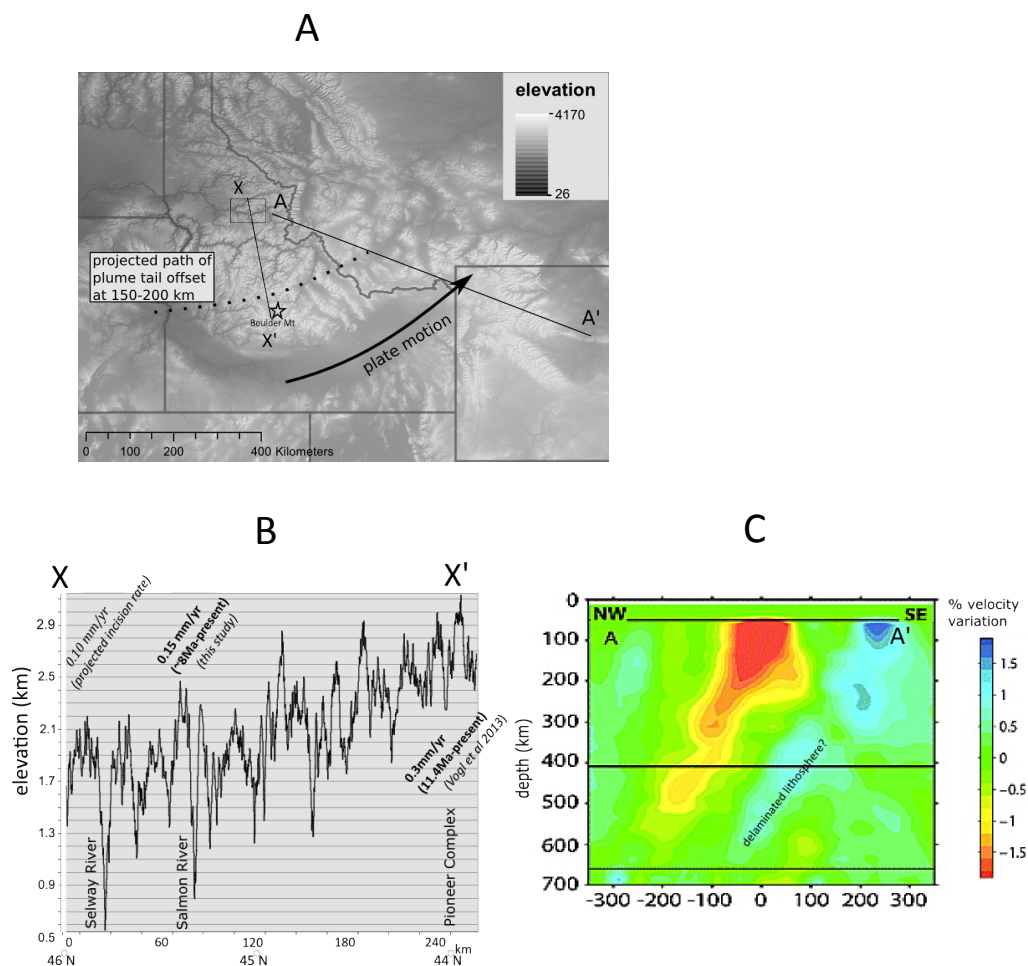


Figure 13: Plume-lithosphere dynamics. [A] The path of the Yellowstone hotspot-track (black arrow) and plume tail offset at the base of the Wyoming Craton (dotted line) due to relative plate motion. [B] Topography and site specific incision rates. Topography was measured along transect X-X' in figure B. Incision rates from the Selway River are interpolated from canyon depths measured within the box in figure A. Higher Topography correlates with greater uplift rates to the south. The trend in incision rates correlates with the trend in topography as the landscape achieves steady-state. [D] Tomography of P-wave velocities along A-A' (Yuan and Dueker, 2005). Low velocity zones (red) mark the location of the plume column. High velocity zones (blue) are interpreted as downwelling lithospheric slabs (Yuan and Dueker, 2005).

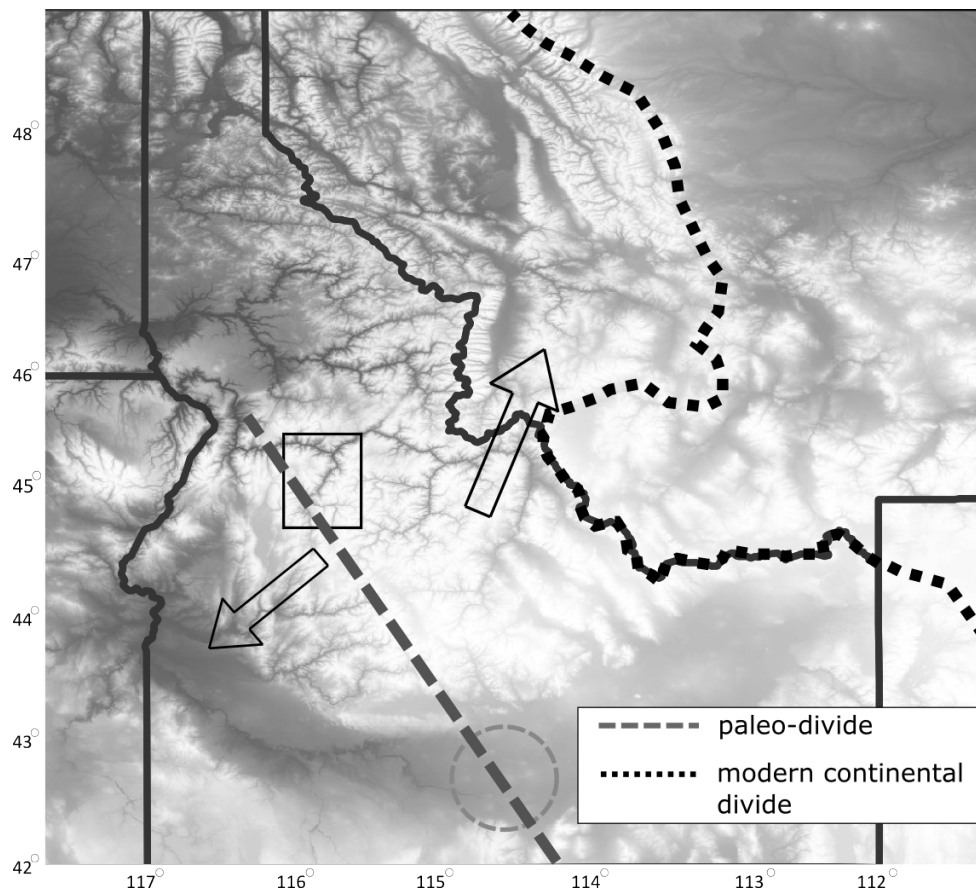


Figure 14: Drainage divide migration from 9 Ma to the present. Note that topography is representative of modern topography and not topography 9 Ma. The modern continental divide is shown by the black dashed line. Note that the drainage divide for the Salmon river is the Idaho-Montana border. Our study area is confined to the black box. The dashed Circle represents the location of the Twin Falls eruptive center, the location of the paleo-continental divide over the Snake River Plain at 9 Ma (Beranek et al., 2006). The orientation of the paleo-divide north of the Snake River Plain is recreated to be perpendicular to plate motion and parallel to the modern continental divide. The arrows show paleo-drainage directions at 9 Ma determined from detrital zircon provenance (Beranek et al., 2006).